THE ASTROPHYSICAL JOURNAL, 487:536–554, 1997 October 1

SOFT X-RAY PROPERTIES OF FLAT-SPECTRUM RADIO QUASARS

RITA M. SAMBRUNA
NRC Research Associate, NASA/GSFC, Code 662, Greenbelt, MD 20771; sambruna@attilla.gsfc.nasa.gov
Received 1997 January 9; accepted 1997 May 9

ABSTRACT

We report the soft X-ray properties of 41 flat-spectrum radio quasars (FSRQs), derived by cross-correlating literature blazar samples with the *ROSAT* PSPC archive of pointed observations. The redshifts of the sources span the range $z = 0$–3. The 0.1–2.4 keV spectra of FSRQs are well described by a single power law modified by column densities of neutral gas consistent with Galactic values. Spectral flattening/steepening at the lower energies is present in only 4/41 and 2/41 sources, respectively. The *ROSAT* photon indices of FSRQs span a wide range, $0.5 \lesssim \Gamma \lesssim 2.5$, and have a measurable intrinsic dispersion; only in part is the spread of slopes due to a redshift effect. The rest-frame *ROSAT* spectral indices of FSRQs are statistically indistinguishable from low-energy peaked BL Lacs and flatter than high-energy peaked BL Lacs, although with several FSRQs having soft X-ray spectra as steep as HBLs. Similarly, while the bulk of FSRQs are intrinsically X-ray brighter than both types of BL Lacs, the X-ray luminosity distributions of the three classes have a large overlap. The *ROSAT* spectra of 13 FSRQs are steeper than measured with the *Einstein* IPC (0.3–4.5 keV), indicating a flat tail emerging at $\approx$1–2 keV at rest-frame energies. We find a trend for blazars with stronger optical emission lines to be more γ-ray–loud and to have flatter X-ray-to-γ-ray continua, possibly supporting external Compton scattering models as the primary generation mechanisms of the high-energy continuum in these objects.

For several FSRQs repeatedly observed with *ROSAT* on timescales of weeks to years, flux variations not larger than a factor of 2 have been detected, with more typical variability amplitude on the order of 10%–30%, and with no accompanying spectral changes. This appears to be in contrast to the less luminous BL Lacs, which are generally characterized by large-amplitude X-ray flux changes, usually accompanied by correlated spectral variations.

Subject headings: BL Lacertae objects: general — quasars: general — radio continuum: galaxies — X-rays: galaxies

1. INTRODUCTION AND MOTIVATION

Blazars are a fascinating class of Active Galactic Nuclei characterized by highly luminous and rapidly variable continuum emission at all observed frequencies from radio to γ-rays (e.g., Urry & Padovani 1995). They include both flat-spectrum radio quasars (FSRQs) and BL Lacertae objects (BL Lacs). While both blazar classes share the properties of a nonthermal continuum, by definition FSRQs have strong and broad (rest-frame equivalent width $EW_r \gtrsim 5$ Å) optical emission lines, while in BL Lacs the optical lines are weak ($EW_r \lesssim 5$ Å) or absent. FSRQs have higher bolometric luminosities than BL Lacs (Sambruna, Maraschi, & Urry 1996) and can exhibit signs of thermal activity possibly related to an accretion disk in their optical and UV spectra (Smith et al. 1986, 1988) in contrast to BL Lacs, which have smooth continua. The broad emission lines are intrinsically brighter in FSRQs than in BL Lacs (Padovani 1992), although with distributions spanning a similar range in luminosity over four decades (Scarpa & Falomo 1997).

The continuum emission mechanisms in FSRQs and BL Lacs appear to be similar (Sambruna et al. 1996). The radio through UV/soft X-ray continuum is produced via synchrotron emission from plasma in relativistic motion in a jet oriented close to the line of sight (Urry & Padovani 1995, and references therein), while a likely origin of the continuum from hard X-rays to γ-rays is inverse Compton scattering of seed photons either internal to the jet (Maraschi, Ghisellini, & Celotti 1992), or from the disk/broad line region (Dermer, Schlickeiser, & Mastichiadis 1992; Sikora, Begelman, & Rees 1994; Ghisellini & Madau 1996). The synchrotron and inverse Compton components overlap in the X-rays, yielding a variety of observational behaviors in different blazar classes (Sambruna et al. 1996; Padovani & Giommi 1996). Since the balance between the two spectral components is related to the physical conditions of the source, a detailed study of the X-ray continuum and its variability in different classes of blazars can provide interesting constraints on the theoretical models.

The X-ray spectra of BL Lacs have been relatively well studied at both soft (0.1–2.4 keV) and hard ($\gtrsim$2 keV) X-rays. At medium to soft energies, the X-ray spectra are in general well described by a single power-law model absorbed at lower energies by a column density of neutral gas consistent with the Galactic value (Worrall & Wilkes 1990; Urry et al. 1996), with different slopes in different subclasses. High-energy peaked BL Lacs (HBLs), whose radio to X-ray energy distributions peak at UV/soft X-rays (Giommi, Ansari, & Micol 1995), have steep X-ray continua, with a trend of steeper spectra in the lower intensity state; spectral convexity is observed in some individual sources and for the cumulative spectra of HBLs (Sembay et al. 1993; Sambruna et al. 1994a, 1994b). Low-energy peaked BL Lacs (LBLs), whose peak power is typically at IR/optical frequencies, are on average flatter in soft X-rays than HBLs (Lamer, Brunner, & Staubert 1996; Padovani & Giommi 1996; Urry et al. 1996), with an opposite trend of steeper X-ray continua during the higher intensity state (Cappi et al. 1994; Madejski et al. 1996; Urry et al. 1996). These properties are consistent with a scenario where the X-ray band in HBLs is dominated by the high-energy tail of the synchrotron emission, while a flat inverse Compton component emerges at approximately a few keV in LBLs

(Ulrich, Maraschi, & Urry 1997). The X-ray and multifrequency spectral properties of HBLs and LBLs can be interpreted in terms of different intrinsic physical parameters, with HBLs being dominated by high magnetic fields and/or electron energies, while radiation densities play a more important role in LBLs (Sambruna et al. 1997).

On the contrary, there is scant information about the shape of the X-ray emission of FSRQs and its variability, except for a few individual cases (3C 273, Leach, McHardy, & Papadakis 1995; 3C 345, Unwin et al. 1997). Class studies at medium-hard X-rays with the *Einstein* IPC (0.3–4.5 keV) and at energies $\gtrsim 2$ keV with *EXOSAT* and *GINGA* (Ohashi et al. 1989; Worrall & Wilkes 1990; Sambruna et al. 1994a, 1994b) concluded that FSRQs have on average flatter continua than BL Lacs at medium-hard X-rays, although on the basis of small samples and/or limited sensitivity. Recent studies of FSRQs with *ROSAT* seem to confirm that also at soft X-rays strong emission line blazars have flatter X-ray continua than both HBLs and LBLs (Brunner et al. 1994; Urry et al. 1996). However, the latter studies dealt with a small sample (eight objects) of FSRQs mostly at high redshifts ($z > 1$), and a bias toward flat X-ray slopes could arise due to the known correlation between the X-ray photon index and redshift for radio-loud quasars (Schartel et al. 1996). Clearly, larger samples of FSRQs are needed to study the X-ray spectral properties of these blazars better.

In this paper we present the spectra of 41 FSRQs observed in pointed mode with the *ROSAT* Position Sensitive Proportional Counter (PSPC) in 0.1–2.4 keV. The sample was derived from cross-correlating the *ROSAT* database of pointed observations with published blazar lists, and includes objects in the redshift range $z = 0$–3. The aim of this work is twofold. The first goal is to study in detail the shape of the soft X-ray continuum emission of FSRQs and its variability. The improved sensitivity of the PSPC in the 0.1–2.4 keV energy range allows us to detect and quantify possible excess absorption over Galactic (e.g., Elvis et al. 1994) as well as excess counts at softer energies (as in 3C 273, Leach et al. 1995). Both can significantly affect the shape of the primary nuclear continuum in the limited bandpass of the PSPC, which clarifies the importance of a careful spectral analysis. Several FSRQs of our sample have been repeatedly observed with *ROSAT*, allowing a detailed study of their long-term flux and spectral variability. Typically, long exposures combined with high signal-to-noise ratio also allow a search for flux variability on shorter ($\sim$hours) timescales in several objects.

As mentioned above, previous comparisons of the *ROSAT* spectra of blazar classes were limited to small samples of FSRQs mostly at redshifts higher than for both HBLs and LBLs. An additional motivation for this work is thus expanding the sample of FSRQs to include more objects in a larger redshift range, in order to perform a proper comparison of the X-ray properties of different blazar classes. Of the 41 FSRQs studied here, 25 are at $z < 1$, in a range of redshifts matching BL Lacs, allowing a comparison of their X-ray continua at similar rest-frame energies. A similar work has been performed independently by Padovani, Giommi, & Fiore (1997) on the basis of the spectral information derived from hardness ratios for a larger samples of FSRQs. Finally, we present accurate spectral fits for each object in the sample.

The paper is structured as follows. The sample and the data analysis are described in §§ 2 and 3, respectively. Results of the *ROSAT* spectral analysis and study of the X-ray variability are given in § 4, which also includes a study of the long-term X-ray variability (§ 4.3). The comparison of the *ROSAT* slopes of FSRQs with those of HBLs and LBLs is given in § 5. In § 6 the principal observational findings are summarized, while discussion and conclusions follow in §§ 6 and 7, respectively. In the Appendix we comment on the *ROSAT* data of individual objects. Throughout this work $H_0 = 75$ km s^{-1} Mpc^{-1} and $q_0 = 0.5$ are assumed.

2. THE SAMPLE

The sample of FSRQs was derived from cross-correlating literature catalogs with the *ROSAT* PSPC archive. The following FSRQ lists were used: The 2 Jy sample of FSRQs (Padovani 1992), derived from the radio catalog of Wall & Peacock (1985); the Pearson & Readhead (1988) sample, including only the 29 sources with compact radio emission and flat spectra; the Impey & Tapia (1988) blazar sample; the S5 sample (Kühr et al. 1981; Pauliny-Toth et al. 1981); the Angel & Stockman (1980) compilation of confirmed strong-emission line blazars. A few (seven) additional flat-spectrum, strong emission-line (equivalent width > 5 Å) sources from Kühr & Schmidt (1990) were also considered, together with PKS 0521−365, a candidate FSRQ of the 2 Jy sample (Urry & Padovani 1995).

A total of 93 FSRQs was derived from the above lists; 41 of these objects were observed with the *ROSAT* PSPC (0.1–2.4 keV). All 41 objects were detected with a significance of 3 σ or more over 2 orders of magnitude in X-ray flux. This sample of 41 FSRQs is by no means complete in a statistical sense.

The sources are listed in Table 1, together with their alternate names and redshifts (cols. [2] and [3]), the amount of Galactic absorption along the line of sight, $N_{\rm H}^{\rm Gal}$ (col. [4]), and the sample to which they belong (col. [5]; overlaps are not indicated). Columns (6)–(9) report information about the *ROSAT* PSPC observations, including, respectively, the observation request number (ROR), the starting date of the pointing, the exposure, and the total source (background-subtracted) counts in the energy range 0.1–2.4 keV. For six sources (0016+731, 0153+744, 0256+075, 0615+820, 0711+356, and 2203−188) less than 100 counts were obtained in single exposures. The last column of Table 1 lists the source hardness ratios, (H − S)/(H + S), where H are the counts in the energy range 0.11–0.40 keV (PI channels 11–40) and S are the counts in 0.41–2.48 keV (PI channels 41–245), following Urry et al. (1996). Some of the *ROSAT* observations were previously published by other authors; for consistency these data have been reextracted here.

Several FSRQs in Table 1 were observed repeatedly with the PSPC. Their multiple observations have been designated with sequential numbers in parenthesis after the target's name in order of increasing observing date, e.g., 0208−512 (1) indicates the first observation of 0208−512, 0208−512 (2) its second pointing, and so on. 3C 279 and 3C 273 were extensively observed with *ROSAT* as part of multifrequency campaigns (Maraschi et al. 1994; Grandi et al. 1996). The *ROSAT* PSPC observation log of 3C 279 and the results of the spectral analysis are presented separately in Table 2. For the log and analysis of the *ROSAT* data of 3C 273 we refer the reader to Leach et al. (1995); only the

TABLE 1

ROSAT PSPC Observations of FSRQs

Source (1)	Other Name(s) (2)	z (3)	N_H^{Gal} ($\times 10^{20}$ cm^{-2}) (4)	Sample[a] (5)	ROR Number (6)	Start Date (7)	Exposure (s) (8)	Counts[b] (9)	Hardness Ratio (10)
0016+731 (1)[c]	...	1.781	21.1	S5	700494	92 Mar 10	6018	51 ± 9	1.21 ± 0.30
(2)[c]					700847	92 Jul 29	5243	52 ± 9	0.99 ± 0.23
0133+476	OC 457	0.859	11.4	WP	700839	92 Aug 12	4036	286 ± 18	0.94 ± 0.04
0153+744	...	2.338	24.7	S5	700138	91 Mar 16	7870	89 ± 12	1.13 ± 0.14
0208−512[d] (1)	...	1.003	2.4	WP	701159	93 May 28	2698	634 ± 27	0.31 ± 0.05
(2)					701160	93 May 29	4026	1038 ± 34	0.35 ± 0.03
(3)					701161	93 May 30	1811	472 ± 23	0.32 ± 0.05
(4)					701163	93 Jun 1	2735	667 ± 28	0.30 ± 0.04
(5)					701164	93 Jun 2	1780	446 ± 23	0.33 ± 0.05
(6)					701167	93 Jun 5	2701	708 ± 28	0.40 ± 0.04
(7)					701168	93 Jun 6	2534	696 ± 28	0.39 ± 0.04
(8)					701158	93 Jun 7	2149	577 ± 26	0.44 ± 0.05
(9)					701157	93 Jun 8	2220	577 ± 26	0.42 ± 0.04
(10)					701156	93 Jun 9	1952	500 ± 24	0.35 ± 0.05
0212+735	...	2.367	41.0[e]	WP	700139	91 Feb 16	7210	287 ± 18	1.02 ± 0.04
0256+075	...	0.893	10.1	KS	701421	93 Aug 15	3028	28 ± 7	0.81 ± 0.35
0403−132	OF−105	0.571	4.3	WP	700271	91 Mar 1	10879	1501 ± 42	0.71 ± 0.03
0405−123	OF−109	0.574	3.7	WP	701072	92 Aug 27	4758	348 ± 50	0.39 ± 0.02
0438−436 (1)	...	2.852	1.3	WP	700028	91 Feb 19	10725	579 ± 28	1.23 ± 0.06
(2)					700867	92 Sep 19	10506	476 ± 25	1.09 ± 0.05
0521−365[d]	...	0.055	3.4	WP	701179	92 Aug 29	4845	3652 ± 63	0.55 ± 0.02
0528+134[d] (1)	OG 147	2.07	39.0[e]	WP	700059	91 Mar 16	3791	261 ± 17	1.03 ± 0.04
(2)					900340	92 Sep 22	4514	391 ± 21	1.02 ± 0.03
0615+820 (1)[c]	...	0.710	5.8	S5	700492	93 Feb 22	7401	79 ± 11	0.94 ± 0.14
(2)[c]					701060	93 Mar 11	3024	43 ± 9	0.98 ± 0.32
0637−752	...	0.654	5.6	WP	700790	92 May 26	1357	112 ± 12	0.91 ± 0.05
0711+356	OI 318	1.620	7.0	PR	701355	93 Sep 26	2496	27 ± 7	0.90 ± 0.36
0736+017	OI 61	0.191	15.0[e]	WP	700064	91 Apr 3	3296	394 ± 20	1.01 ± 0.03
0804+499[d]	OJ 508	1.430	4.6	PR	700846	92 Oct 27	3000	145 ± 14	0.90 ± 0.07
0836+710[d] (1)	4C71.07	2.160	2.83	WP	700493	92 Mar 23	6993	5178 ± 73	0.70 ± 0.01
(2)					701061	92 Nov 2	5026	1890 ± 45	0.73 ± 0.02
0906+430	3C 216	0.670	1.4	WP	700329	91 Nov 14	23561	1038 ± 36	0.43 ± 0.04
0923+392 (1)	4C39.25	0.698	1.6	WP	700067	91 Apr 15	2524	855 ± 31	0.02 ± 0.04
(2)					700505	92 May 1	3796	1338 ± 38	−0.04 ± 0.03
(3)					700848	93 Apr 22	3585	1503 ± 40	0.03 ± 0.03
(4)					700849	93 Apr 24	4147	1763 ± 44	0.00 ± 0.03
(5)					700850	93 Apr 26	4568	1976 ± 46	0.01 ± 0.02
(6)					700851	93 Apr 28	5136	2128 ± 48	−0.02 ± 0.02
(7)					700852	93 Apr 30	5423	2275 ± 50	0.02 ± 0.02
0945+408	4C40.24	1.252	1.5	PR	701400	93 Nov 10	2704	171 ± 15	0.08 ± 0.09
0954+554[d]	4C55.17	0.8	0.9	WP	701401	93 Nov 8	4472	384 ± 22	−0.32 ± 0.06
1034−293	...	0.312	3.9	IT	700201	92 Feb 2	3975	347 ± 20	0.56 ± 0.06
1039+811	...	1.260	2.5	S5	700141	91 Mar 17	6570	485 ± 24	0.42 ± 0.05
1055+018	4C01.28	0.888	3.45	WP	701198	93 Jun 5	4324	383 ± 22	0.43 ± 0.06
1150+497	4C49.22	0.334	2.1	AS	701073	92 Dec 1	6610	1851 ± 44	0.20 ± 0.02
1150+812 (1)	...	1.250	4.5	S5	700496	92 Apr 8	8575	227 ± 17	0.91 ± 0.08
(2)					701059	92 Oct 30	9504	230 ± 17	0.90 ± 0.06
1223+026[d]	3C 273	0.158	1.8	WP	700191	91 Dec 14	6243	36,272 ± 125	0.18 ± 0.00
1253−055[d]	3C 279	0.537	2.2	WP	...[f]	...[f]	...[f]	...[f]	...[f]
1335−127	OP−158	0.539	4.8	IT	700203	92 Feb 1	3615	496 ± 24	0.92 ± 0.04
1510−089[d]	OR−017	0.361	7.6	WP	700854	92 Aug 17	5153	945 ± 32	0.86 ± 0.02
1611+343[d] (1)	OS 319	1.403	1.4	WP	700842	92 Aug 30	3651	427 ± 22	0.04 ± 0.06
(2)						93 Jan 17	3153	380 ± 21	0.36 ± 0.06
1633+382[d]	4C38.41	1.814	1.0	WP	700841	92 Aug 30	5781	1183 ± 36	0.24 ± 0.03
1642+398 (1)	3C 345	0.594	0.9	WP	150014	90 Jul 19	4090	1137 ± 37	−0.07 ± 0.03
(2)					700428	92 Jan 16	3899	1875 ± 66[g]	0.04 ± 0.04
(3)					700869	92 Sep 1	4219	2023 ± 47	0.16 ± 0.02
(4)					700843	92 Sep 3	2857	1142 ± 44[g]	0.00 ± 0.04
(5)					799870	93 Mar 6	5986	1675 ± 43	0.08 ± 0.03
(6)					700428	93 Jul 19	946	278 ± 27[g]	−0.04 ± 0.11
1732+389	...	0.976	3.1	KS	701417	93 Oct 1	6658	105 ± 12	0.83 ± 0.12
1921−293	...	0.352	7.8	AS	900338	93 Mar 24	32600	8802 ± 95	0.90 ± 0.005
1928+738	4C73.18	0.302	5.1	WP	700142	91 Mar 14	8451	2286 ± 49	0.94 ± 0.01
2134+004	OX 57, PHL 61	1.936	5.1	WP	700817	92 Dec 2	6035	473 ± 22	0.86 ± 0.03
2155−152	OX−192	0.672	3.7	KS	701420	93 Nov 16	9940	867 ± 32	0.51 ± 0.04
2203−188	OY−106	0.618	2.5	WP	800196	92 May 10	8733	62 ± 12	0.19 ± 0.29
2223−052 (1)	3C 446	1.404	5.3	WP	800143	91 Nov 20	4825	353 ± 21	0.91 ± 0.05
(2)					900337	93 May 23	15626	1313 ± 38	0.86 ± 0.02

TABLE 1—*Continued*

Source (1)	Other Name(s) (2)	z (3)	N_H^{Gal} ($\times 10^{20}$ cm^{-2}) (4)	Sample[a] (5)	ROR Number (6)	Start Date (7)	Exposure (s) (8)	Counts[b] (9)	Hardness Ratio (10)
2251+158[d] (1).....	3C 454.3	0.859	13.1[d]	WP	700076	91 Nov 28	6413	1603 ± 40	0.95 ± 0.01
(2).....					700759	92 May 27	8154	3425 ± 57	0.96 ± 0.01
(3).....					900339	92 Dec 16	22156	7508 ± 88	0.94 ± 0.01

[a] (WP) 2 Jy sample, Wall & Peacock 1985; (S5) S5 survey, Pauliny-Toth et al. 1981; (IT) Impey & Tapia 1988; (KS) 1 Jy sample, Kühr & Schmidt 1990; (PR) Pearson & Readhead 1989; (AS) Angel & Stockman 1980.
[b] Source counts in the spectral extraction cell (§ 2) in the 0.1–2.4 keV energy range.
[c] Observations (1) and (2) were combined in the spectral analysis.
[d] Sources detected with *CGRO* EGRET at MeV energies (Thompson et al. 1995).
[e] Total atomic + molecular Galactic column density in the direction to the source.
[f] The complete log of the *ROSAT* observations is given in Table 2.
[g] Corrected for rib obscuration, following Unwin et al. 1997.

longest archival exposure has been used here.

All observations were performed in pointed mode, with the source in the center of the field of view. Three sources were off-axis in a few pointings, which were centered on other targets: 3C 345 during ROR 700428, 700843, and 700428 (off-axis angles ∼20′, 28′, and 14′, respectively), 2203−188 during ROR 800196 (off-axis by ∼8′), and 2223−052 during ROR 800143 (off-axis by ∼13′). During the offset pointings part of the counts from 3C 345 were lost since the source was partially covered by the support ribs of the PSPC. The counts listed in Table 1 are corrected for this effect, using the correction factors of Unwin et al. (1997). The signal-to-noise ratio of the observations in Table 1 ranges from 4 to 290, with median ∼22.

The Galactic column densities in column 4 of Table 1 were taken from Elvis, Lockman, & Wilkes (1989), Lockman & Savage (1995), and Murphy et al. (1996) when available (typical uncertainties on these values are $\sim 1 \times 10^{19}$ cm^{-2}), or from Stark et al. (1992) otherwise (uncertainties $\sim 1 \times 10^{20}$ cm^{-2}). The sources 0212+735,

TABLE 2

ROSAT PSPC Observations of 3C 279 ($z = 0.537$; Galactic $N_H = 2.2 \times 10^{20}$ cm^{-2})

				N_H Fixed (Galactic Value)			N_H Free		
ROR Number	Date	Exposure (s)	Counts	Γ	χ_r^2/dof	$F_{1\,keV}$ (μJy)	N_H ($\times 10^{20}$ cm^{-2})	Γ	χ_r^2/dof
700305.....	92 Jan 2	8513	4465 ± 68	1.80 ± 0.04	0.97/122	1.23 ± 0.04	$2.80^{+0.28}_{-0.41}$	$1.98^{+0.09}_{-0.07}$	0.92/121
700075.....	92 Jan 3	4230	2194 ± 48	1.87 ± 0.06	1.21/74	1.16 ± 0.05	$2.64^{+0.64}_{-0.39}$	$1.97^{+0.21}_{-0.11}$	1.19/73
700978.....	92 Dec 27	3228	1266 ± 37	1.81 ± 0.07	1.02/46	0.91 ± 0.06	$3.03^{+0.74}_{-0.65}$	$2.07^{+0.23}_{-0.22}$	0.95/45
700979.....	92 Dec 28	3431	1531 ± 40	1.88 ± 0.07	0.94/54	1.00 ± 0.05	$3.08^{+0.50}_{-0.78}$	$2.16^{+0.15}_{-0.03}$	0.89/53
700980.....	92 Dec 29	3688	1499 ± 40	1.82 ± 0.07	1.12/55	0.93 ± 0.05	$2.90^{+0.64}_{-0.56}$	$2.04^{+0.21}_{-0.15}$	1.07/54
700981.....	92 Dec 30	3711	1517 ± 40	1.83 ± 0.07	1.26/56	0.92 ± 0.05	$3.71^{+0.66}_{-0.63}$	$2.30^{+0.22}_{-0.21}$	0.98/55
700982.....	92 Dec 31	1867	747 ± 29	1.86 ± 0.09	0.96/29	0.89 ± 0.07	$2.17^{+1.15}_{-0.50}$	$1.83^{+0.34}_{-0.18}$	1.00/28
701101.....	93 Jan 2	3894	1574 ± 41	1.76 ± 0.06	0.68/61	0.96 ± 0.05	$2.88^{+0.82}_{-0.44}$	$1.96^{+0.28}_{-0.11}$	0.60/60
701102.....	93 Jan 2	1454	588 ± 25	1.88 ± 0.11	1.27/23	0.89 ± 0.08	$2.26^{+1.28}_{-0.77}$	$1.88^{+0.44}_{-0.27}$	1.32/22
701104.....	93 Jan 2	3181	1232 ± 36	1.92 ± 0.08	1.00/45	0.84 ± 0.05	$3.21^{+0.74}_{-0.68}$	$2.24^{+0.25}_{-0.23}$	0.89/44
701105.....	93 Jan 2	3489	1405 ± 39	1.86 ± 0.07	0.98/52	0.90 ± 0.05	$3.15^{+0.70}_{-0.61}$	$2.16^{+0.24}_{-0.17}$	0.90/51
701106.....	93 Jan 3	3939	1623 ± 42	1.83 ± 0.07	1.13/59	0.93 ± 0.05	$2.53^{+0.56}_{-0.53}$	$1.93^{+0.20}_{-0.18}$	1.13/58
700985.....	93 Jan 3	1835	775 ± 28	1.84 ± 0.09	0.82/30	0.96 ± 0.07	$2.33^{+1.16}_{-0.60}$	$1.87^{+0.39}_{-0.21}$	0.84/29
701109.....	93 Jan 3	3213	1336 ± 38	1.80 ± 0.07	1.78/48	0.93 ± 0.05	$2.97^{+0.70}_{-0.65}$	2.05 ± 0.23	1.74/47
701110.....	93 Jan 3	3518	1446 ± 39	1.79 ± 0.10	0.62/52	0.96 ± 0.07	$2.72^{+0.77}_{-0.95}$	$1.93^{+0.31}_{-0.20}$	0.63/51
701111.....	93 Jan 4	2006	827 ± 30	1.91 ± 0.10	0.87/31	0.91 ± 0.07	$2.40^{+0.81}_{-0.74}$	$1.96^{+0.29}_{-0.27}$	0.89/30
701113.....	93 Jan 4	1973	833 ± 30	1.81 ± 0.09	0.71/33	0.98 ± 0.07	$2.44^{+0.72}_{-0.85}$	$1.86^{+0.27}_{-0.19}$	0.73/32
701114.....	93 Jan 4	3200	1298 ± 36	1.84 ± 0.07	0.89/48	0.92 ± 0.05	$2.80^{+0.73}_{-0.67}$	$2.02^{+0.12}_{-0.23}$	0.88/47
701115.....	93 Jan 4	1752	744 ± 29	1.77 ± 0.10	0.60/29	0.98 ± 0.09	$2.26^{+1.21}_{-0.53}$	$1.77^{+0.41}_{-0.19}$	0.60/28
701116.....	93 Jan 4	3800	1525 ± 41	1.86 ± 0.07	1.40/57	0.90 ± 0.05	$3.02^{+0.64}_{-0.57}$	$2.13^{+0.20}_{-0.17}$	1.33/56
701120.....	93 Jan 5	3594	1573 ± 41	1.83 ± 0.06	1.06/55	1.00 ± 0.05	$2.84^{+0.60}_{-0.63}$	$2.03^{+0.20}_{-0.13}$	1.04/54
700987.....	93 Jan 5	2814	1207 ± 36	1.79 ± 0.08	0.89/45	1.00 ± 0.05	$3.47^{+0.83}_{-0.65}$	$2.17^{+0.28}_{-0.15}$	0.68/44
701119.....	93 Jan 5	3213	1329 ± 38	1.88 ± 0.07	1.16/49	0.92 ± 0.05	$3.05^{+0.74}_{-0.56}$	$2.16^{+0.25}_{-0.03}$	1.06/48
700988.....	93 Jan 6	2002	858 ± 31	1.86 ± 0.08	1.23/33	0.94 ± 0.07	$3.20^{+0.58}_{-0.56}$	$2.14^{+0.19}_{-0.18}$	1.02/59
700990.....	93 Jan 8	3860	1805 ± 43	1.81 ± 0.06	1.51/63	1.06 ± 0.05	$3.37^{+0.46}_{-0.69}$	$2.17^{+0.14}_{-0.04}$	1.38/62
700991.....	93 Jan 9	3500	1593 ± 41	1.73 ± 0.07	0.96/56	1.08 ± 0.05	$3.07^{+0.61}_{-0.62}$	$1.98^{+0.22}_{-0.16}$	0.88/55
700992.....	93 Jan 10	3897	1701 ± 43	1.78 ± 0.07	1.05/63	1.03 ± 0.05	$2.45^{+0.56}_{-0.53}$	1.86 ± 0.19	1.06/62
700993.....	93 Jan 11	3384	1433 ± 40	1.74 ± 0.07	1.26/53	0.98 ± 0.05	$2.76^{+0.92}_{-0.47}$	$1.91^{+0.30}_{-0.15}$	1.22/52
700994.....	93 Jan 12	4003	1652 ± 41	1.77 ± 0.07	1.22/60	0.97 ± 0.05	$2.26^{+0.85}_{-0.34}$	$1.77^{+0.30}_{-0.12}$	1.24/59
700995.....	93 Jan 13	1969	824 ± 30	1.84 ± 0.10	1.29/32	0.93 ± 0.07	$2.82^{+0.94}_{-0.86}$	$2.04^{+0.33}_{-0.31}$	1.30/31

0528+134, 0736+017, and 2251+158 lie behind dark molecular clouds. For these objects an equivalent column density of molecular hydrogen was estimated from the integrated CO emission line intensity along the line of sight (Liszt & Wilson 1993), assuming the conversion factor of Bania, Marscher, & Barvainis (1991). The Galactic N_H listed in Table 1 for these four sources is the total hydrogen column density (atomic plus molecular).

The large majority of sources are well studied at other wavelengths. A small subgroup of 12 objects (flagged in Table 1) were detected at γ-rays with the *CGRO* EGRET experiment (Thompson et al. 1995).

3. *ROSAT* DATA ANALYSIS

Source counts were extracted (using IRAF v.2.10.2) from a circle centered on the source position with radius 1′ for the sources with $\lesssim$1000 counts, above which the background is dominant in the radial profiles. When more than 1000 counts were detected, a source circle with radius 2′ was necessary in order to collect the softest photons and avoid the "ghost-image" effect (Nousek & Lesser 1993). The background was evaluated in a concentric annulus of inner and outer radii $\sim$2′ and 3′ for sources with less than 1000 counts, and of radii 3′ and 4′ for sources with more than 1000 counts, excluding serendipitous sources if necessary. A vignetting correction was applied in the few cases where the source was observed off-axis.

3.1. *Timing Analysis*

We checked for flux variability on timescales equal to or shorter than the *ROSAT* exposure times by applying the Kolmogorov-Smirnov and the χ^2 tests. For the objects with 100 counts or more, light curves were extracted and rebinned on timescales $\gtrsim$400 s, to avoid spurious variability due to the satellite wobble. Depending on the source strength and on the type of variability, either test can be more sensitive.

Significant flux variability was detected for the 1992 January 2 observation of 3C 279 (ROR 700305; Table 2) and the 1992 April 8 observation of 1150+812 (ROR 700496; Table 1). In both cases, the KS probability that the cumulative photon distribution is uniform is $\lesssim$1%. Inspection of the light curves shows that the *ROSAT* flux of 3C 279 decreased by 15% in $\sim$2 months, while for 1150+812 an increase of the flux by a factor 1.8 in $\sim$1 month is present.

For the remaining objects no variability was detected within the *ROSAT* exposures with either a KS or χ^2 test. This could be due to an intrinsic lack of large-amplitude variability on shorter timescales, or to the limited temporal range spanned by the *ROSAT* exposures. As discussed in Urry et al. (1996), our extensive simulations show that, for a source with 100 (1000) counts, the KS and χ^2 tests would pick up trends with $\gtrsim$50% (5%) amplitude variability, or a factor 2.7 (1.3) flare at 99% confidence. On the other hand, the satellite wobble and the relatively short exposures limit our sensitivity to timescales on the order of about a few hours in most cases. Variability on long timescales is discussed later (§ 4.3).

3.2. *Spectral Analysis*

Spectra were extracted in 256 pulse invariant channels only for the objects with $\gtrsim$100 net counts in Table 1. The spectra were rebinned on the energy range 0.14–2.1 keV (PI channels 14–201), where the spectral response is best known, in order to have at least 20 counts in each new bin, to validate the use of the χ^2 statistics. The spectral fits were performed within XSPEC v.9.01 using the response matrices pspcb-gain1-256 for observations taken in high-gain mode (before 1991 October 14) and pspcb-gain2-256 for low-gain mode (after 1991 October 14). Each pair of observations for the weak sources 0016+731 and 0615+820 were co-added in the spectrum extraction procedure in order to increase the signal-to-noise ratio.

As a first, simple approximation the *ROSAT* spectra were fitted with a single power-law model modified by photoelectric absorption at low energies. Absorption was parameterized in terms of the neutral hydrogen column density, N_H (in cm^{-2}), using the Morrison & McCammon (1983) cross section with the abundances of elements heavier than hydrogen fixed to solar. For all sources, we performed spectral fits with the column density N_H fixed to the Galactic value in the direction to the object, which gives tighter constraints on the spectral index and the flux density at 1 keV. For all sources except the weak quasars 0016+731, 0615+820, 0637−752, and 1732+389 we also performed fits with free N_H.

In some cases (see below) evidence for a spectrum more complex than a single power law with Galactic absorption is present. We thus fitted the PSPC data with more complex spectral models, including a broken power law, a power law plus a blackbody, and a power law plus an absorption edge. The statistical improvements of these fits with respect to the single power-law fits were decided on the basis of the *F*-test, with a threshold for the minimal confidence of $P_F = 95\%$. The χ^2 probability, P_{χ^2}, was also used, assuming a fit is acceptable when $P_{\chi^2} \gtrsim 5\%$.

4. RESULTS OF SPECTRAL ANALYSIS

4.1. *Single Power-law Fits*

Table 3 lists the spectral parameters derived from the single power-law fits together with their 90% confidence errors (for one parameter of interest, $\Delta\chi^2 = 2.7$). Columns (2)–(4) report the photon index Γ, the reduced χ^2 per degrees of freedom (dof), and the acceptance probability P_{χ^2}, respectively, for the fixed (Galactic) N_H fits. Columns (5)–(8) give the same for the free-N_H fits. The flux densities at 1 keV in column (9) were obtained from the fixed-N_H fits, unless otherwise stated. Repeated observations of the same sources are reported in Table 3, using the convention in Table 1. For 3C 279 the fits to the *ROSAT* observations are presented separately in Table 2, and only average values and 1 σ dispersions are given in Table 3 (no significant variability of the spectral parameters have been found for this object; see § 4.3).

The sources 0153+744, 0256+075, 0711+356, and 2203−188 were detected with too few counts (<100) to allow spectral analysis. In Table 3 for these objects we report flux densities at 1 keV derived assuming a single power law with Galactic absorption and photon index $\Gamma = 1.96$ or $\Gamma = 1.67$ depending on whether their redshift is below or above 1, respectively (§ 4.4).

From Table 3 it is apparent that the single power law with Galactic column density provides a good fit for most objects. However, this model is unacceptable ($P_{\chi^2} < 5\%$) in a number of cases, including 0208−512(5), 0438−436(1), 3C 273, 1633+382, 1928+738, and 2223−052(2). In the

TABLE 3

SINGLE POWER-LAW FITS TO THE *ROSAT* PSPC SPECTRA OF FSRQs

	N_H FIXED (GALACTIC VALUE)			N_H FREE				N_H FIXED
OBJECT (1)	Γ (2)	χ^2_r/dof (3)	P_{χ^2} (%) (4)	N_H ($\times 10$ cm^{-2}) (5)	Γ (6)	χ^2_r/dof (7)	P_{χ^2} (%) (8)	Flux Density at 1 keV (μJy) (9)
0016+731	$1.43^{+1.01}_{-1.19}$	0.10/2	91.4	...	...	...	...	0.05 ± 0.01
0133+476	$1.92^{+0.38}_{-0.40}$	0.80/11	64	$7.50^{+6.17}_{-3.6}$	~ 1.57	0.72/10	71	0.30 ± 0.03
0153+744	...	...	...	...	...	...	...	0.6 ± 0.2
0208−512(1).....	1.91 ± 0.13	0.60/24	93.7	$1.22^{+0.91}_{-0.75}$	$1.50^{+0.34}_{-0.32}$	0.40/23	99.5	$0.54^{+0.03}_{-0.07}$
(2).....	1.87 ± 0.09	1.24/39	14.5	$1.95^{+0.76}_{-0.71}$	$1.73^{+0.26}_{-0.23}$	1.24/38	14.7	0.58 ± 0.04
(3).....	1.89 ± 0.14	1.40/18	12.0	$1.85^{+0.72}_{-1.15}$	$1.73^{+0.25}_{-0.47}$	1.38/17	13.5	0.58 ± 0.06
(4).....	1.99 ± 0.11	0.76/26	80.3	$2.45^{+0.85}_{-0.97}$	$2.01^{+0.29}_{-0.35}$	0.78/25	77.0	0.53 ± 0.05
(5).....	$1.95^{+0.13}_{-0.15}$	1.87/17	1.6	$1.89^{+1.16}_{-1.15}$	$1.77^{+0.43}_{-0.42}$	1.95/16	1.3	0.53 ± 0.06
(6).....	1.85 ± 0.10	1.16/28	25.5	$2.55^{+0.69}_{-1.08}$	$1.90^{+0.25}_{-0.39}$	1.20/27	22.0	0.60 ± 0.05
(7).....	1.79 ± 0.11	1.17/28	24.5	$1.65^{+0.70}_{-0.75}$	$1.54^{+0.24}_{-0.25}$	1.10/27	32.8	0.64 ± 0.05
(8).....	1.73 ± 0.13	0.98/22	48.6	$2.30^{+1.18}_{1.04}$	$1.70^{+0.38}_{-0.37}$	1.03/21	42.1	0.66 ± 0.06
(9).....	1.79 ± 0.12	0.81/23	72.2	$2.70^{+0.90}_{-1.14}$	$1.88^{+0.22}_{-0.38}$	0.85/22	66.4	0.62 ± 0.06
(10)	$1.88^{+0.02}_{-0.12}$	0.70/19	82.3	$1.76^{+1.24}_{-1.00}$	$1.67^{+0.40}_{-0.38}$	0.68/18	83.5	0.59 ± 0.06
0212+735	$0.66^{+0.58}_{-0.60}$	1.46/10	14.5	32 (<110)	~ 0.51	1.60/9	11.0	0.26 ± 0.04
0256+075	...	...	...	...	...	...	...	<0.05
0403−132	1.73 ± 0.09	0.95/56	58.2	$3.86^{+0.84}_{-0.79}$	$1.78^{+0.22}_{-0.23}$	0.96/55	56.0	0.40 ± 0.02
0405−123	2.33 ± 0.06	1.12/79	21.8	$3.11^{+0.70}_{-0.41}$	$2.15^{+0.22}_{-0.13}$	1.10/78	25.5	1.16 ± 0.05
0438−436(1).....	$0.61^{+0.13}_{-0.15}$	1.75/23	1.4	$6.80^{+4.59}_{-2.13}$	$1.72^{+0.42}_{-0.37}$	0.70/22	84.5	0.15 ± 0.01
(2).....	$0.51^{+0.20}_{-0.77}$	0.61/18	89.5	$6.64^{+12.97}_{-3.81}$	$1.63^{+0.76}_{-0.78}$	0.24/17	99.9	0.13 ± 0.02
0521−365	1.92 ± 0.05	0.92/119	77.5	$3.83^{+0.60}_{-0.34}$	$2.04^{+0.17}_{-0.10}$	0.89/118	79.8	2.01 ± 0.07
0528+134(1).....	$1.45^{+0.40}_{-0.42}$	1.04/18	41.0	$85.4^{+64.6}_{-40.4}$	$3.35^{+2.35}_{-1.85}$	1.02/17	43.2	1.65 (<7.2)[a]
(2).....	$1.35^{+0.34}_{-0.35}$	1.29/18	18.2	$93.7^{+56.3}_{-39.7}$	$3.61^{+2.19}_{-1.64}$	1.02/17	43.2	2.48 (<9.6)[a]
0615+820	$1.68^{+0.50}_{-0.68}$	0.70/3	55.8	...	...	...	...	0.04 ± 0.008
0637−752	$1.45^{+0.42}_{-0.49}$	0.52/3	67.0	...	...	...	...	0.31 ± 0.06
0711+356	...	...	...	...	...	...	...	0.04 ± 0.03
0736+017	$2.45^{+0.29}_{-0.30}$	0.87/15	59.8	$20.04^{+22.32}_{-9.37}$	$2.82^{+0.76}_{-0.44}$	0.87/14	59.2	0.57 ± 0.05
0804+499	$1.39^{+0.37}_{-0.48}$	0.63/4	64.1	$5.63^{+12.27}_{-4.78}$	$1.58^{+1.49}_{-1.18}$	0.79/3	50.1	0.16 ± 0.03
0836+710(1).....	1.38 ± 0.04	1.14/142	11.8	$3.63^{+0.44}_{-0.35}$	$1.59^{+0.12}_{-0.09}$	1.00/141	48.4	2.12 ± 0.06
(2).....	1.37 ± 0.07	1.18/67	14.6	$3.87^{+0.97}_{-0.47}$	$1.64^{+0.24}_{-0.13}$	1.00/66	47.7	1.07 ± 0.05
0906+430	1.41 ± 0.09	0.91/39	63.0	$1.44^{+0.68}_{-0.59}$	1.43 ± 0.24	0.93/38	59.3	0.10 ± 0.008
0923+392(1).....	2.18 ± 0.09	1.25/31	16.8	$1.47^{+0.68}_{-0.59}$	$2.09^{+0.29}_{-0.25}$	1.28/30	14.0	0.52 ± 0.05
(2).....	2.27 ± 0.07	1.02/46	43.5	$1.93^{+0.49}_{-0.63}$	$2.37^{+0.10}_{-0.14}$	1.01/45	45.3	0.52 ± 0.04
(3).....	2.15 ± 0.06	1.03/51	34.0	$1.81^{+0.74}_{-0.38}$	$2.19^{+0.29}_{-0.13}$	1.04/50	40.0	0.68 ± 0.05
(4).....	2.22 ± 0.06	0.90/56	56.0	$2.19^{+0.47}_{-0.59}$	$2.42^{+0.18}_{-0.14}$	0.89/55	70.4	0.65 ± 0.04
(5).....	2.18 ± 0.06	0.92/63	63.4	$1.75^{+0.55}_{-0.50}$	$2.21^{+0.17}_{-0.20}$	0.93/62	63.3	0.68 ± 0.04
(6).....	2.22 ± 0.06	0.86/63	76.0	$1.63^{+0.54}_{-0.36}$	$2.20^{+0.21}_{-0.11}$	0.87/62	75.7	0.63 ± 0.04
(7).....	2.15 ± 0.06	1.24/66	8.8	$2.36^{+0.36}_{-0.54}$	$2.40^{+0.13}_{-0.11}$	1.18/65	15.2	0.68 ± 0.04
0945+408	1.96 ± 0.23	1.00/5	41.6	1.14 (<3)	$1.81^{+0.78}_{-0.66}$	1.20/4	30.0	0.11 ± 0.02
0954+554	2.14 ± 0.15	0.84/13	59.6	$0.41^{+1.11}_{-0.41}$	$1.93^{+0.26}_{-0.30}$	0.89/12	55.7	0.10 ± 0.02
1034−293	$1.96^{+0.21}_{-0.22}$	1.67/13	6.0	$1.92^{+0.97}_{-1.29}$	$1.41^{+0.33}_{-0.39}$	1.14/12	32.0	0.24 ± 0.03
1039+811	1.83 ± 0.13	0.78/19	73.0	$2.44^{+0.68}_{-1.46}$	$1.79^{+0.24}_{-0.36}$	0.82/18	68.4	0.18 ± 0.02
1055+018	2.20 ± 0.16	0.99/14	45.6	$2.79^{+1.17}_{-1.44}$	$1.93^{+0.44}_{-0.45}$	0.97/13	47.8	0.21 ± 0.03
1150+497	2.14 ± 0.05	0.93/67	63.3	$2.46^{+0.58}_{-0.44}$	$2.25^{+0.23}_{-0.08}$	0.92/66	66.0	0.55 ± 0.03
1150+812(1).....	$1.45^{+0.29}_{-0.33}$	0.77/8	63.0	$5.20^{+5.04}_{-2.52}$	$1.55^{+0.67}_{-0.55}$	0.80/7	58.7	0.09 ± 0.008
(2).....	$1.22^{+0.32}_{-0.36}$	0.66/8	72.7	$4.85^{+6.81}_{-2.72}$	$1.27^{+0.74}_{-0.60}$	0.72/7	65.5	0.09 ± 0.008
3C 273	2.01 ± 0.01	1.23/183	1.9	1.64 ± 0.10	1.94 ± 0.04	1.17/182	6.0	11.70 ± 0.13
3C 279	1.83 ± 0.05[b]	...	...	2.85 ± 0.42[b]	2.02 ± 0.15[b]	...	...	0.97 ± 0.08[b]
1335−127	$1.63^{+0.15}_{-0.17}$	0.95/20	52.4	$6.82^{+3.84}_{-1.36}$	$2.00^{+0.53}_{-0.29}$	0.73/19	79.2	0.45 ± 0.04
1510−089	$1.89^{+0.16}_{-0.17}$	1.30/26	9.8	$6.20^{+2.2}_{-1.7}$	1.70 ± 0.35	1.29/37	11.2	0.66 ± 0.05
1611+343(1).....	1.52 ± 0.13	0.40/14	97.6	$1.62^{+1.29}_{-0.87}$	$1.58^{+0.47}_{-0.34}$	0.40/13	97.6	0.27 ± 0.03
(2).....	1.94 ± 0.13	1.56/16	7.05	$0.72^{+0.78}_{-0.58}$	$1.63^{+0.57}_{-0.30}$	1.51/15	9.2	0.20 ± 0.02
1633+382	1.58 ± 0.07	1.67/41	0.5	$2.08^{+0.96}_{-0.44}$	$1.96^{+0.33}_{-0.16}$	1.43/40	3.8	0.39 ± 0.03
3C 345(1)	1.98 ± 0.08	1.50/44	1.8	$0.82^{+0.28}_{-0.54}$	$1.96^{+0.14}_{-0.36}$	1.52/43	1.6	0.38 ± 0.03
(2).....	1.75 ± 0.08	0.92/44	64.0	$1.15^{+0.67}_{-0.45}$	$1.85^{+0.31}_{-0.15}$	0.93/43	60.3	0.98 ± 0.08[c]
(3).....	1.73 ± 0.05	0.97/66	70.4	$1.86^{+0.49}_{-0.42}$	2.12 ± 0.11	0.75/65	93.4	0.83 ± 0.05

TABLE 3—*Continued*

	N_H Fixed (Galactic Value)			N_H Free				N_H Fixed
Object (1)	Γ (2)	χ_r^2/dof (3)	P_{χ^2} (%) (4)	N_H ($\times 10$ cm^{-2}) (5)	Γ (6)	χ_r^2/dof (7)	P_{χ^2} (%) (8)	Flux Density at 1 keV (μJy) (9)
(4).....	1.81 ± 0.09	1.06/33	38.9	$1.17^{+0.64}_{-0.57}$	$1.95^{+0.26}_{-0.30}$	1.09/32	33.3	0.85 ± 0.08[c]
(5).....	1.78 ± 0.06	0.97/55	62.2	$1.41^{+0.48}_{-0.44}$	$1.99^{+0.20}_{-0.19}$	0.91/54	66.2	0.46 ± 0.03
(6).....	1.84 ± 0.26	0.57/6	78.6	...	...	...		0.61 ± 0.18[c]
1732+389	$1.58^{+0.35}_{-0.41}$	0.41/2	66.4	...	...	...	...	0.05 ± 0.009
1921−293	1.89 ± 0.05	1.06/166	27.6	$8.84^{+0.58}_{-0.64}$	$2.02^{+0.08}_{-0.06}$	1.02/165	41.4	1.06 ± 0.02
1928+738	1.73 ± 0.07	2.11/83	$<10^{-6}$	$11.67^{+2.04}_{-1.47}$	$2.33^{+0.21}_{-0.17}$	0.83/82	86.5	1.17 ± 0.08[a]
2134+004	$1.59^{+0.16}_{-0.19}$	0.88/18	60.4	$6.34^{+3.61}_{-1.91}$	$1.82^{+0.48}_{-0.37}$	0.85/17	63.5	0.26 ± 0.02
2155−152	2.17 ± 0.10	0.81/32	76.7	$4.57^{+1.39}_{-0.82}$	$2.42^{+0.38}_{-0.22}$	0.72/31	87.3	0.22 ± 0.02
2203−188	...	...	...	...	...	...	...	0.007 ± 0.006
2223−052(1).....	$1.66^{+0.19}_{-0.21}$	0.56/14	89.7	$7.26^{+3.27}_{-2.08}$	$2.00^{+0.45}_{-0.41}$	0.41/13	96.7	0.25 ± 0.02
(2).....	1.69 ± 0.10	1.51/48	1.3	$7.45^{+1.51}_{-0.99}$	$2.09^{+0.28}_{-0.18}$	1.26/47	10.9	0.27 ± 0.01
2251+158(1).....	1.90 ± 0.15	0.97/60	53.4	$9.76^{+5.14}_{-2.33}$	$1.67^{+0.38}_{-0.30}$	0.95/59	58.5	1.16 ± 0.05
(2).....	1.90 ± 0.10	0.93/115	69.2	$12.05^{+6.00}_{-2.74}$	$1.83^{+0.39}_{-0.25}$	0.93/114	69.0	1.93 ± 0.05
(3).....	2.07 ± 0.07	1.05/150	51.2	$10.61^{+1.18}_{-0.94}$	$1.87^{+0.13}_{-0.08}$	1.00/149	48.9	1.55 ± 0.03

[a] From free-N_H fits.
[b] Average parameter and 1 σ dispersion (from Table 2).
[c] Corrected for rib obscuration (see Unwin et al. 1997).

case of 0208−512(5) and 1633+382 the inspection of the residuals shows the presence of local χ^2 fluctuations whose interpretation is not obvious. No significant improvement is obtained if N_H is allowed to vary (Table 3) nor fitting more complex models to the data. In the following, for 0208−512(5) and 1633+382 we will continue to use the spectral index from the fixed-N_H fit.

In the remaining cases, 0438−436(1), 3C 273, 1928+738, and 2223−052(2), the fit with free-N_H is acceptable and is significantly improved ($P_F \gtrsim 99\%$) with respect to the fixed-N_H fit. The fitted column density is larger than Galactic for 0438−436(1), 1928+738, and 2223−052(2), while it is lower than Galactic for 3C 273. Figure 1 shows the confidence contours for N_H and Γ obtained from the free-N_H fits to these spectra. The vertical solid and dashed lines represent the Galactic N_H and its 90% confidence range, respectively. In 0438−436, 1928+738, and 2223−052 the excess N_H is significant at more than 99% confidence. In 3C 273 the fitted column density is lower than Galactic at $\sim$90% confidence.

Also shown in Figure 1 are the contours for 0528+134, 0836+710 (joint fit for the spectra of both observations of this source), and 1034−293. In these objects, although the fit with a single power-law model is formally acceptable, a significant improvement of the χ^2 is obtained when the column density is left free to vary. The fitted column density of 0836+710 is in excess of the Galactic column density of Murphy et al. (1996) at $\sim$99% confidence. While the column density of 0528+134 is consistent with values in excess to Galactic, the uncertainties in Figure 1 for this source are too large to draw any conclusion (*ASCA* spectra of 0528+134 confirm excess absorption; see Appendix). A fitted column density lower than Galactic is indicated for 1034−293 at $\sim$98% confidence (Fig. 1).

4.2. *More Complex Spectral Fits*

As discussed above, in a number of sources the fitted X-ray column density differs from the Galactic value, being larger in five cases and lower in two cases (Fig. 1). Since the Galactic value is the minimum column density in the direction to an X-ray source, fits yielding values of N_H lower than Galactic are not acceptable and are usually interpreted as evidence for the presence of excess counts at the softer energies. On the other hand, because of the limited sensitivity and bandpass of the PSPC, an intrinsically convex continuum can be mimicked by excess absorption at the lower energies. We thus looked for models that can reproduce spectral flattening/soft excess with the column density fixed to Galactic. Below we summarize the results of these more complex spectral fits.

4.2.1. *Excess Absorption*

We fitted the *ROSAT* data of the sources apparently exhibiting extra absorption with a broken power law plus N_H^{Gal}. Not surprisingly, this model provides a fit significantly better than the power law plus Galactic N_H, and statistically equivalent to the single power law with free N_H, due to the limited bandpass of the PSPC. In general, the fits with the convex broken power law provide zero or even negative low-energy photon indices, i.e., an inverted spectrum below the break energy. The implied curvature gradients, $\Delta\Gamma \equiv \Gamma_{\rm hard} - \Gamma_{\rm soft} \gtrsim 1$, are unusually strong even when compared to the convex continua of HBLs, for which $\Delta\Gamma \lesssim 0.5$ are measured (Sambruna et al. 1994b). Since there is no immediate physical explanation of such strong curvatures, we have fitted the PSPC data with alternative models.

We considered the possibility that the spectral flattening is due to an absorber located along the line of sight, in addition to the local absorber in the Galaxy. The *ROSAT* data were fitted with a model consisting of a power law plus Galactic absorption plus a column density at a redshift z_a free to vary (e.g., Elvis et al. 1994). In no case was it possible to constrain z_a, due to the low signal-to-noise ratio. In the case of 2223−052, fixing z_a to the redshift of the intervening damped Lyα system at $z \sim 0.5$ (Lanzetta et al. 1991) provides an acceptable fit (Appendix).

We note here, for future reference, that for the steep sources 0736+017 and 1150+497 the fits in Table 3 suggest

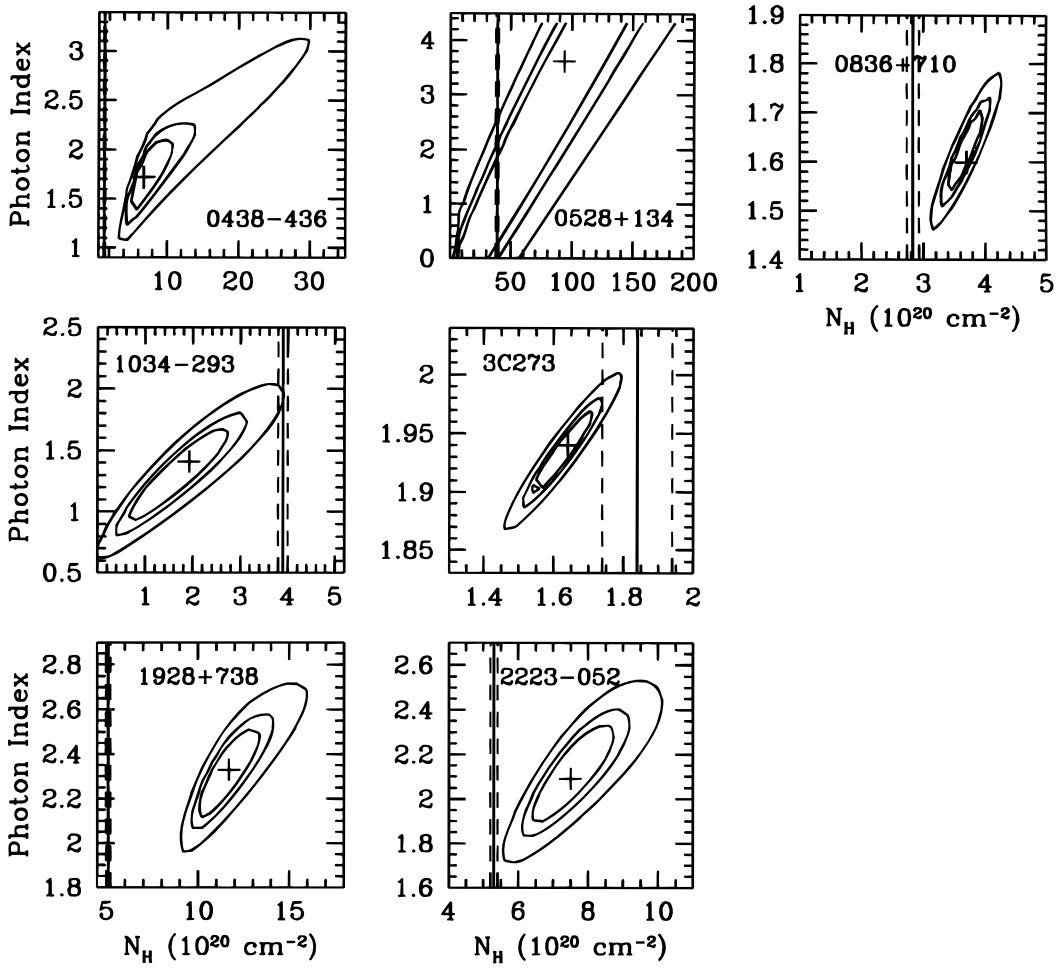

FIG. 1.—Confidence contours for the photon index Γ and column density N_H from the fits with an absorbed power-law model to the *ROSAT* PSPC data of seven FSRQs. The cross marks the best-fit, and the contours enclose regions of spectral parameters at 68%, 90%, and 99% confidence level ($\Delta\chi^2 = 2.3$, 4.6, and 9.3, respectively). The vertical solid line marks the Galactic column density in the direction to each source, and the dashed lines are its nominal 90% confidence range. Four sources, 0438−436, 0836+710, 1928+738, and 2223−052 show evidence for excess column density over Galactic at more than 99% confidence, while for two sources (1034−293 and 3C 273) the fitted column density is lower than Galactic at 90%–98% confidence.

a convex spectrum. In fact, the fits with free N_H yield a steeper photon index than the fits with Galactic N_H in both cases, and a somewhat higher column density. Fitting the data with a broken power law yields a convex continuum, but the fit is not statistically improved with respect to the power-law fits.

4.2.2. *Soft Excess*

Only two sources exhibit column densities lower than Galactic, 3C 273 and 1034−293 (Leach et al. 1995; Maraschi et al. 1995), indicating the presence of excess soft counts. We modeled the soft excess flux both in terms of a broken power law plus Galactic column density, and by adding a thermal model (blackbody) to the fits with a single power law plus Galactic N_H. In addition, since excess soft flux in the lower channels can be mimicked by the presence of lower energy absorption features in the limited bandpass of the PSPC, we also fitted the *ROSAT* spectra of 3C 273 and 1034−293 with a power-law plus edge model. The results are described in the Appendix. We find that for 3C 273 the three models provide statistically similar descriptions of the spectrum, while for 1034−293 only the power-law plus edge model provides an improved fit to the data.

A number of objects in the sample, i.e., 0637−752, 0736+017, 1510−089, 3C 345, and 2251+158, exhibit signs of thermal activity in their optical/UV spectra, usually in the form of excess unpolarized flux (Wills et al. 1980; Smith et al. 1986, 1988; Siemiginowska et al. 1995). We checked whether a thermal component is present in their *ROSAT* spectra by fitting the data with a power-law plus blackbody model. In all cases the slope was fixed at the value determined at higher X-ray energies (assuming no spectral variability) from IPC or, when available, from *EXOSAT* ME or *GINGA* data. In general, the addition of the blackbody is not necessary from a statistical perspective, and the fit converges to zero normalization for the thermal component. A possible exception is 3C 345 (Appendix). We conclude that in general the thermal optical and UV emission does not extend into the soft X-ray spectra of FSRQs.

In summary, evidence for spectral flattening/soft excess at *ROSAT* lower energies is found only for a very low fraction (3%–4%) of the PSPC spectra of our sample of FSRQs. We conclude that in general the *ROSAT* spectra of FSRQs are well represented by a single power law with Galactic absorption.

4.3. *Long-term X-Ray Variability of FSRQs*

The FSRQs 0208−512, 0923+392, 3C 279, and 3C 345 were observed with *ROSAT* at several epochs (Tables 1 and 2), allowing a detailed study of their flux and spectral variability on timescales of days to years. In addition, 3C 273 was

also monitored repeatedly (Leach et al. 1995), and we refer to the latter authors for the study of the light curve.

Figures 2*a*–2*d* show the *ROSAT* light curves of 0208−512, 0923+392, 3C 279, and 3C 345 (*bottom panels*) together with the plots of the *ROSAT* photon index (from the fixed-N_H fits) versus time (*top panels*). The light curves in Figure 2 were sampled on various timescales from days to years. The γ-ray blazar 0208−512 was observed daily from 1993 May 28 to June 9, exhibiting flux changes with maximum amplitude 13% on a timescale of 9 days (Fig. 2*a*); there is a hint of spectral variability, in the sense of flattening spectrum with increasing intensity. 0923+392 was observed once in 1991 April and 1992 May, and then every two days from 1993 April 22 to 30; its *ROSAT* flux (Fig. 2*b*) increased by 20% in 2 years, with no accompanying spectral changes, and remained constant during the 10 days monitoring in 1993. *ROSAT* pointed at 3C 279 first in 1992 January 2 and 3, and then again about a year later in 1992 December 27, when the flux was a factor of 1.3 (30%) fainter. The source was then monitored on an almost daily basis for 18 days, during which the intensity remained nearly constant, with a modest ($\sim$13% flux amplitude change) flare occurring in $\sim$1 week as a major event. At no time is there evidence for significant spectral changes. 3C 345 was observed with *ROSAT* first in 1990 July, when its flux was at a low level, and then in 1992 January and September, when the flux was a factor $\approx$2 higher, with a flatter spectrum; however, a similar drop in flux $\sim$6 months later was not accompanied by spectral changes. The X-ray variability amplitude in 3C 279 and 3C 345 tracks the variability at radio-millimeter frequencies (Grandi et al. 1996; Unwin et al. 1997).

The *ROSAT* light curve of 3C 273 shows flux variations of 8% on timescales of 2 days, with a maximum change up to $\sim$20%, and uncorrelated spectral changes (Leach et al. 1995). The study of the X-ray variability in this object is complicated by the presence of the (variable) soft excess.

Each of the following sources, 0438−436, 0528+134, 0836+710, 1611+343, 2223−052, and 2251+158, was observed with *ROSAT* on more than one occasion (although not enough times to plot a long-term light curve). No appreciable flux variations are observed, except in 0836+710, where the flux dropped by a factor of approximately 2 in $\sim$8 months, with no accompanying spectral changes.

In summary, FSRQs repeatedly observed with *ROSAT* show flux variability with amplitudes not larger than a factor of 2 on timescales of months/years, and with little or no accompanying spectral changes. Typical variability amplitudes are of the order of $\sim$30% or less.

4.4. *Distribution of the ROSAT Photon Indices of FSRQs*

Figure 3*a* shows the distribution of the *ROSAT* PSPC spectral indices for the FSRQs (*open histogram*). In general, spectral indices from the fits with fixed (Galactic) N_H were used. In the case of 0438−436(1), 0836+710, 1034−293, 3C 273, 1928+738, and 2223−052(2), where the free-N_H fits are statistically preferred, the values of Γ from these fits were adopted instead. Individual spectral indices from the single observations have been used for the sources observed more than once. In total, 65 spectra for 37 objects were used.

The distribution in Figure 3*a* is wide, with photon indices in the range 0.5–2.5; however, it is highly peaked, with average $\langle\Gamma\rangle = 1.84$ and dispersion $\sigma = 0.31$. Part A of Table 4 summarizes the mean photon indices calculated with various methods. In particular, assuming that the intrinsic parent distribution of the observed *ROSAT* distribution in Figure 3*a* is a Gaussian of center Γ_p and width σ_p, through a maximum likelihood analysis (Worrall 1989) we derive the confidence contours at 90% confidence for Γ_p and σ_p illustrated in Figure 3*b* (*solid line*). FSRQs have a nonzero dispersion, indicating a spread of *ROSAT* slopes.

The large spread of *ROSAT* spectral indices we measure for FSRQs is, at least in part, related to a redshift dependence. It is well known that the *ROSAT* spectral index anticorrelates with the redshift for radio-loud quasars up to $z \sim 2.5$ (Schartel et al. 1996), with a trend of flatter slopes for increasing distances. This is clearly present for the FSRQs of our sample (Fig. 4*a*), with a high correlation significance (Spearman correlation coefficient for two variables $\tau_{12} = -0.466$ corresponding to a correlation probability $P \sim 99.999\%$). A similar trend is present when the slopes are plotted versus the X-ray luminosity (Fig. 4*b*), albeit weaker ($\tau_{12} = -0.245$, $P \sim 95\%$). Using the partial correlation analysis we find that the slope is still strongly anticorrelated with the redshift when the luminosity dependence is subtracted ($\tau_{12,3} = -0.452$, $P \sim 99.98\%$). However, if the effect of the redshift is removed the correlation between the slope and the luminosity changes sign, i.e., the slope and the luminosity become positively correlated ($\tau_{12,3} = 0.231$, $P \sim 93.4\%$). We conclude that for the present sample of FSRQs the observed spread in *ROSAT* slopes is, at least in part, more likely a redshift than a luminosity effect.

We divided the FSRQ sample in two subgroups including sources with redshift $z < 1$ and $z > 1$, respectively. (The threshold $z = 1$ was adopted for comparison with BL Lacs; § 5.1). The distribution of the 29 *ROSAT* spectral slopes for the $z > 1$ FSRQs (hatched histogram in Fig. 3*a*) differs from the distribution of 36 slopes for $z < 1$ FSRQs at 99.7% confidence according to the Kolmogorov-Smirnov test. The simple average slopes of the two distributions (Table 4, part

TABLE 4

A. Average *ROSAT* Photon Indices

Object	Simple $\langle\Gamma\rangle$	Simple σ	Weighted	Maximum Likelihood[a] Γ_p	Maximum Likelihood[a] σ_p
FSRQs.....	1.84	0.31	1.97 ± 0.01	$1.91^{+0.05}_{-0.07}$	$0.20^{+0.05}_{-0.06}$
FSRQs $z < 1$.....	1.96	0.27	2.02 ± 0.01	$1.95^{+0.10}_{-0.06}$	$0.20^{+0.06}_{-0.07}$
FSRQs $z > 1$	1.68	0.30	1.78 ± 0.03	$1.76^{+0.07}_{-0.08}$	$0.09^{+0.09}_{-0.08}$
LBLs.....	2.01	0.45	2.21 ± 0.03	$2.03^{+0.15}_{-0.18}$	$0.33^{+0.14}_{-0.10}$
HBLs	2.41	0.41	2.49 ± 0.01	$2.43^{+0.07}_{-0.16}$	$0.34^{+0.08}_{-0.09}$

B. Average *ROSAT* Luminosities (in ergs s^{-1} Hz^{-1})

Object	Simple $\langle \log L_{1\,keV} \rangle$	Simple σ	Weighted
FSRQs	28.09	0.71	28.105 ± 0.003
FSRQs ($z < 1$).....	27.71	0.56	27.945 ± 0.003
FSRQs ($z > 1$).....	28.60	0.55	29.031 ± 0.007
LBLs	26.86	0.95	...
HBLs.....	27.14	0.56	...

[a] Errors at 90% confidence for two interesting parameters ($\Delta S = 4.6$).

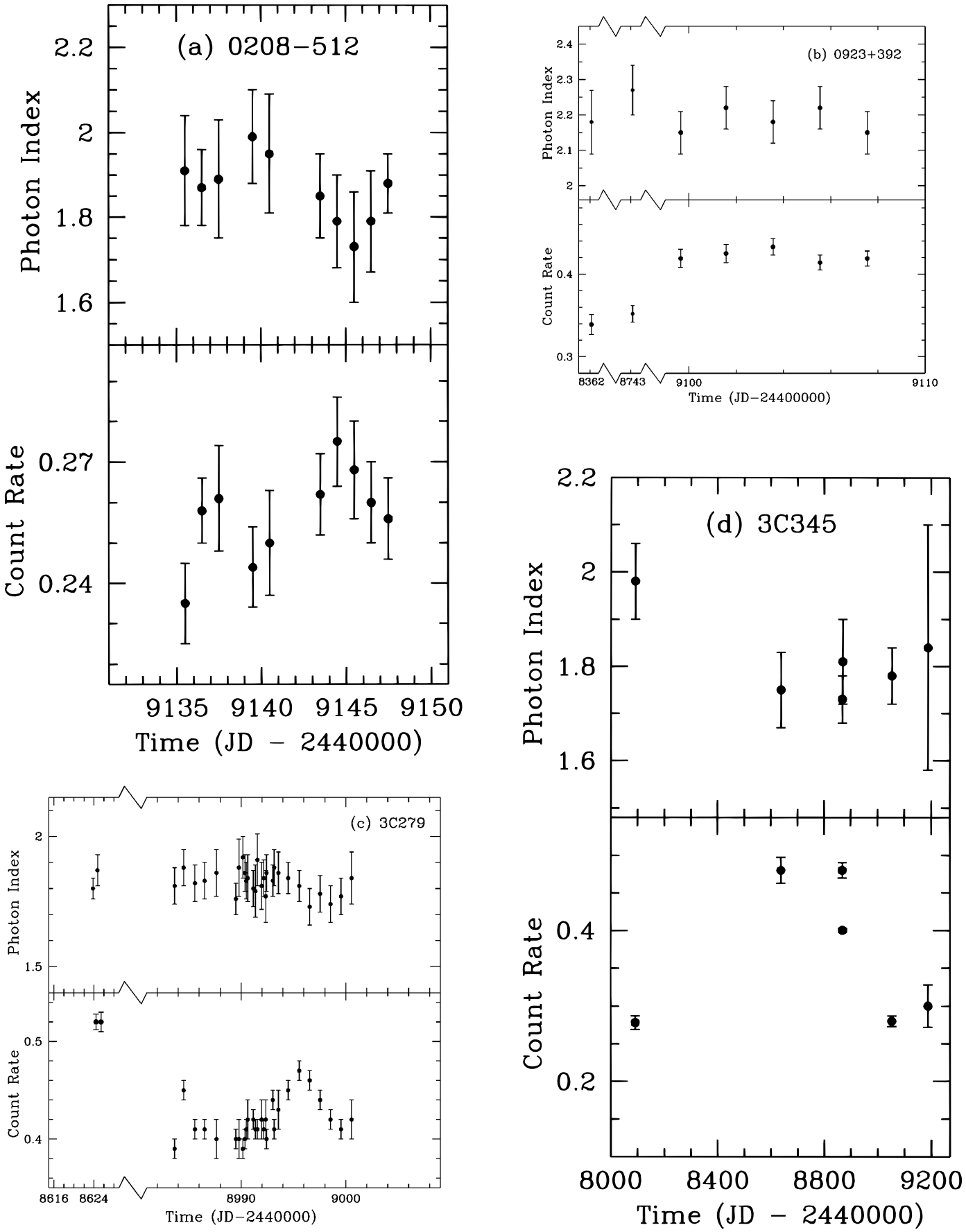

FIG. 2.—X-ray variability of four FSRQs repeatedly observed with *ROSAT*. The *ROSAT* photon indices (*top panels*) and the *ROSAT* count rates in the range 0.1–2.4 keV (*bottom panel*) are plotted vs. the observing date. The slopes are derived from the Galactic N_H fits, with 90% confidence error bars.

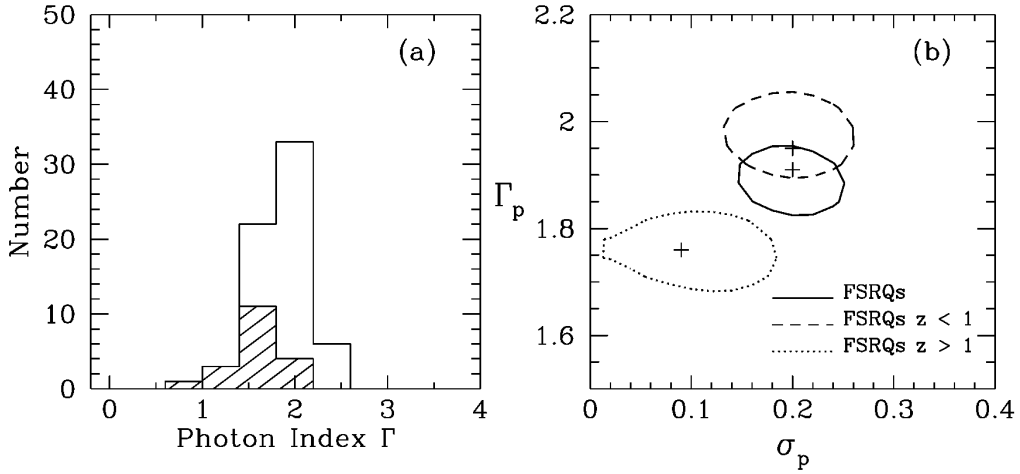

FIG. 3.—(*a*) Distribution of the *ROSAT* spectral indices. *Open histogram:* Distribution for the whole sample of FSRQs. The average photon index is $\langle\Gamma\rangle = 1.84$ with dispersion $\sigma = 0.31$. *Shaded histogram:* Distributions for the subgroups of the 29 FSRQs at $z > 1$, which are clustered at flatter values of the slope. (*b*) Confidence contours at 90% level for two parameters of interest from the maximum likelihood test. The contour for low-z FSRQs enclose a region of steeper slopes and larger dispersion than for high-z FSRQs.

A) differ at 99.99% confidence according to the Student t-test. Figure 3*b* shows the confidence contours for Γ_p and σ_p from the maximum likelihood analysis for low-z FSRQs (*dashed line*) and high-z FSRQs (*dotted line*); while the intrinsic dispersion is now reduced for the $z > 1$ subgroup, the lower-z objects still have a broad distribution of spectral slopes.

In the objects' rest-frame *ROSAT* samples the harder ($\gtrsim$2 keV) X-ray energies for $z > 1$. Figure 3*b* thus leads us to conclude that the hard X-ray continua of FSRQs appear more uniform in spectral shape than at soft X-ray energies, where there is a larger variety of spectral slopes.

4.4.1. *The Subgroup of γ-Ray FSRQs*

The 12 FSRQs flagged in Table 1 were detected at MeV energies with *CGRO* EGRET (Thompson et al. 1995). Their average *ROSAT* slope is 1.76 ($\sigma = 0.26$), which splits into $\langle\Gamma_{z<1}\rangle = 1.94$ ($\sigma = 0.11$) for the seven objects at redshift $z < 1$, and $\langle\Gamma_{z>1}\rangle = 1.50$ ($\sigma = 0.15$) for the five objects at redshift $z > 1$. The average for the γ-ray–emitting FSRQs at low and high redshifts is completely consistent with the average for the corresponding subgroups (Table 4, part A), i.e., the subgroup of γ-ray emitting FSRQs does not have distinctively flatter *ROSAT* spectra. For a discussion of the *ROSAT* spectral properties of a larger sample of γ-ray–loud blazars we refer to Comastri et al. (1997).

4.5. *Comparison with Spectra at Harder X-Ray Energies*

As discussed above, the spread in spectral shapes for FSRQs is in part due to a redshift dependence of the PSPC photon index (Figs. 3 and 4). As suggested by previous authors (e.g., Schartel et al. 1996), a flattening slope with increasing distance may indicate that the rest-frame broad-band X-ray continuum is upward-curved (concave), with a hard tail being progressively redshifted into the *ROSAT* range. An alternative hypothesis is that there is real spectral evolution, with the intrinsic single power-law spectrum flattening with increasing lookback time.

It should be possible in principle to distinguish between these two scenarios by comparing the *ROSAT* spectra with information gathered at higher energies for low-z objects. In the evolutionary hypothesis we should expect to have similar slopes at soft and hard ($\gtrsim$1 keV) energies for the same objects. Vice versa, if the spectrum is intrinsically concave, the hard X-ray slopes should be flatter than in the *ROSAT* range. For the $z < 1$ FSRQs in our sample spectral information at energies harder than *ROSAT* were gathered with the *Einstein* IPC (0.3–4.5 keV) and with missions operating at energies $\gtrsim$2 keV (*EXOSAT* ME, *GINGA*, *ASCA*).

4.5.1. *Comparison ROSAT PSPC/Einstein IPC*

Einstein IPC spectra are available from the archive for 13 low-z FSRQs, including 0403−132, 0405−123, 0521−365, 0637−752, 0736+017, 0923+392, 3C 273, 3C 279, 1510−089, 1335−127, 3C 345, 1921−293, 2251+158. Published spectral slopes for most of these sources are, however, derived from free-N_H fits, and consequently are usually affected by very large uncertainties (Worrall & Wilkes 1990).

In order to derive better constrained photon indices, we reextracted the archival IPC data for the above FSRQs, and fitted the IPC spectra with a single power law plus fixed (Galactic) absorption. The distribution of the IPC photon indices for the 13 FSRQs is shown in Figure 5*a* (*dashed line histogram*). The average slope is $\langle\Gamma_{\rm IPC}\rangle = 1.48$ with $\sigma = 0.37$. The solid line histogram in Figure 5*a* is the distribution of the PSPC slopes for the same 13 FSRQs, which has an average slope $\langle\Gamma_{\rm PSPC}\rangle = 1.94$ and $\sigma = 0.26$. The two distributions differ at 98.5% confidence from the KS test, with the IPC slopes spanning a range of flatter values than the PSPC. The averages for the two distributions differ at 99.9% confidence, according to the Student t-test. The maximum likelihood analysis (Fig. 5*b*) confirms that the 13 FSRQs at $z < 1$ have *ROSAT* slopes steeper than the IPC.

If the difference between the IPC and PSPC slopes is intrinsic, and not due to cross-calibration problems of the two instruments (see Urry et al. 1996 and references therein), the flatter IPC slopes of FSRQs indicate that the *intrinsic* X-ray spectrum of FSRQs is concave, with a flat tail emerging above $\approx$1–2 keV rest-frame energies. A similar comparison for LBLs indicates the onset of a flat tail at hard energies also for the latter objects (Urry et al. 1996).

4.5.2. *Published X-Ray Spectra at Energies* $\gtrsim$ 2 keV

Published spectral information at energies $\gtrsim$2 keV is relatively scarce for FSRQs, because of their X-ray faint-

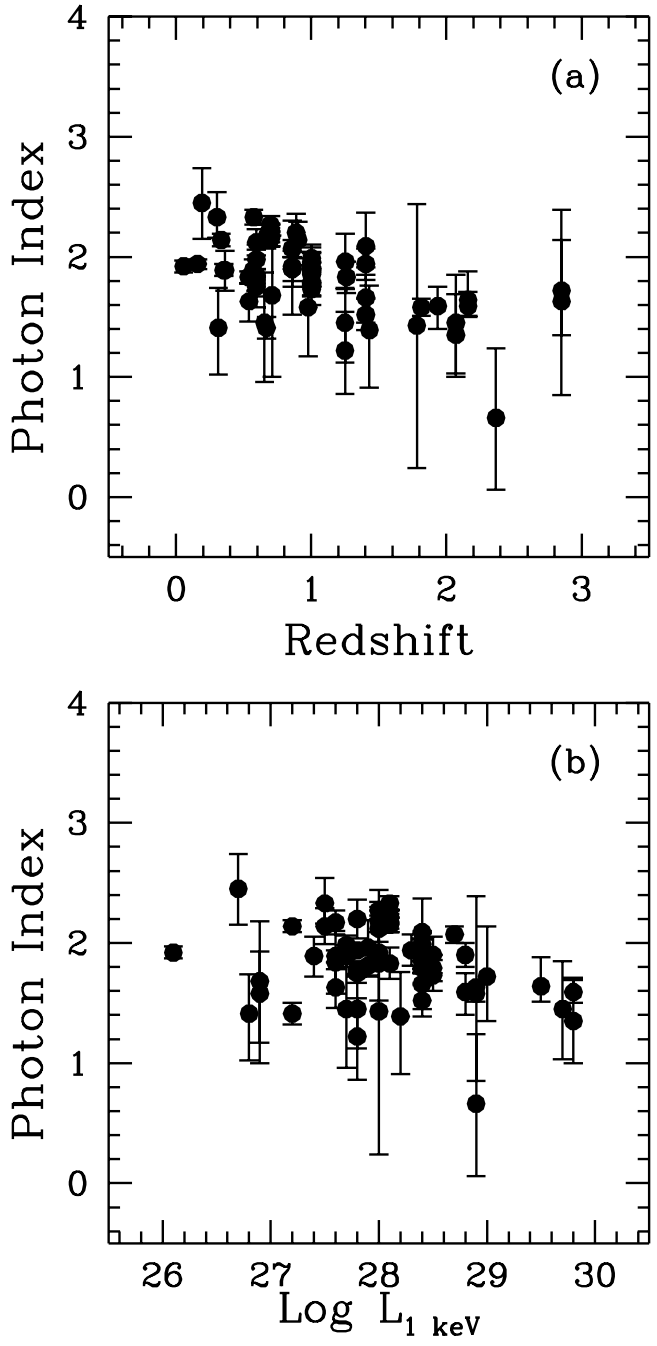

FIG. 4.—Plot of the *ROSAT* photon index of FSRQs vs. (*a*) the redshift and (*b*) the luminosity density at 1 keV. Spectral slopes for each single observation are plotted with their 90% confidence uncertainties. There is a significant (~99.9% confidence) trend of flatter *ROSAT* spectra for more distant sources, in agreement with previous findings for radio-loud quasars (Schartel et al. 1996). Note the dispersion of slopes still present at a given z. A similar trend is apparently present with the luminosities. However, subtracting the common redshift dependence the correlation between the slope and the luminosity changes sign (see text).

ness. Only five low-z FSRQs (0637−752, 3C 273, 3C 279, 3C 345, 2251+158) were observed with *GINGA* (Ohashi et al. 1989), and three more objects (0521−365, 1510−089, and 1928+738) were observed with *EXOSAT* (Brunner et al. 1994; Sambruna et al. 1994b). In general, the published $\gtrsim 2$ keV slopes are affected by large uncertainties (30%–50%). *ASCA* observed a few sources (0521−365, 1510−089, 3C 273, 3C 279); at the time of writing, results have been published for 3C 273 and 3C 279 only (Makino et al. 1996; Reynolds 1997).

A variety of behaviors is indicated when comparing the high-energy slopes to the *ROSAT* ones. Five bright sources (0521−365, 3C 273, 3C 279, 1510−089) have hard X-ray continua flatter than with *ROSAT* by $\Delta\Gamma \sim 0.3$–0.4. In one case (1928+738) the *EXOSAT* spectrum joins smoothly to the *ROSAT* PSPC (Brunner et al. 1994), while in 0637−752 and 2251+158 the *GINGA* continuum is steeper ($\Delta\Gamma \sim 0.5$) than measured with *ROSAT*. The average slope of the continuum above 2 keV for the seven sources is $\langle\Gamma_{\rm hard}\rangle = 1.80$ ($\sigma = 0.41$); the average *ROSAT* slope of the same objects is $\langle\Gamma_{\rm soft}\rangle = 1.90$ ($\sigma = 0.24$). The two average photon indices are very similar, in contrast with the finding above that the IPC spectra of 13 FSRQs in 0.3–4.5 keV are flatter than their *ROSAT* spectra. High-quality broadband spectroscopy is necessary to clarify the shape of the X-ray continua of FSRQs at soft and hard X-rays, an ideal project for the currently operating SAX observatory.

5. COMPARISON WITH BL LAC OBJECTS

We now compare the *ROSAT* spectral properties of FSRQs to those of BL Lacs observed with the PSPC. Large samples of BL Lacs were studied at soft X-rays by Urry et al. (1996), Perlman et al. (1996), and Lamer et al. (1996), with published spectral indices. We have classified the BL Lacs from these works on the basis of their radio-to-X-ray flux ratios, $\alpha_{\rm rx}$, as high-energy peaked BL Lacs (HBLs) when $\alpha_{\rm rx} < 0.8$, and as low-energy peaked BL Lacs (LBLs) when $\alpha_{\rm rx} > 0.8$ (Padovani & Giommi 1996), obtaining a total of 54 HBLs and 26 LBLs. The redshift range of both classes is 0–1.

5.1. *ROSAT Spectral Index*

In Figure 6*a* the distribution of the *ROSAT* photon indices of FSRQs (*solid line*) is compared to HBLs (*dotted line*) and LBLs (*dashed line*). The distribution for the $z > 1$ subgroup of FSRQ is also plotted (*shaded histogram*). The average *ROSAT* photon indices for HBLs and LBLs, $\langle\Gamma_{\rm HBL}\rangle = 2.41$, $\sigma = 0.41$, and $\langle\Gamma_{\rm LBL}\rangle = 2.01$, $\sigma = 0.45$, are in agreement with previous studies (Lamer et al. 1996; Padovani & Giommi 1996; Urry et al. 1996).

In Figure 6*a*, FSRQs and HBLs have spectral index distributions different at $P_{\rm KS} \sim 99.999\%$ confidence according to the KS test, with HBLs having steeper spectra than FSRQs. The distributions for LBLs and FSRQs differ at 93%. Splitting the FSRQs into redshift subgroups, the distributions of $z < 1$ FSRQs and LBLs are not demonstrably different, with $P_{\rm KS} \sim 17\%$. As expected, the distribution for $z > 1$ FSRQs is significantly different ($P_{\rm KS} \sim 99.9\%$) than for both HBLs and LBLs, with flatter slopes (the simple means in part A of Table 4 differ by $\gtrsim 99\%$ according to the Student t-test). Similar conclusions are derived from inspection of Figure 6*b*, where the allowed parameter regions from a maximum likelihood test are shown for the different blazar subclasses.

However, although statistically flatter than HBLs, a number of FSRQs have *ROSAT* spectra as steep as the latter objects. Indeed, note the large overlap of the two observed distributions in Figure 6*a*.

In conclusion, when the *ROSAT* slopes of different blazar classes are compared in similar rest-frame energies, we find that there is no distinction in spectral shapes between LBLs and FSRQs. The latter objects have flatter *ROSAT* spectra

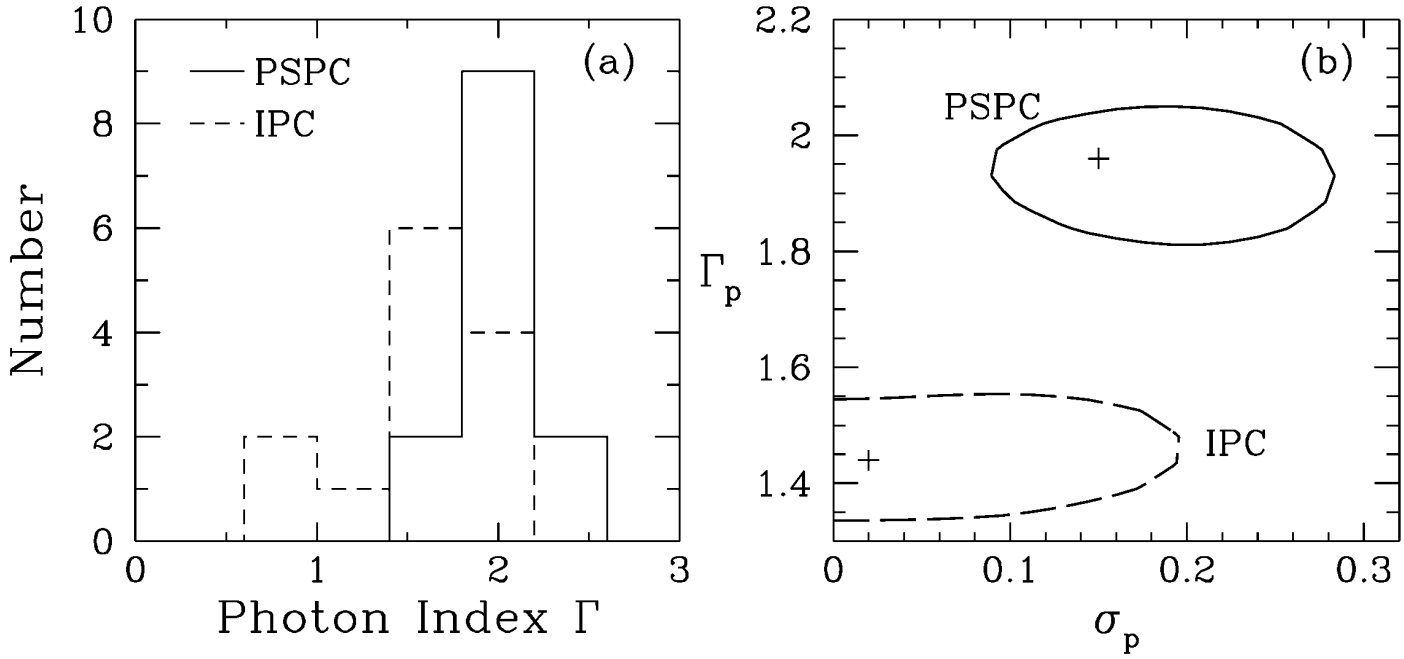

FIG. 5.—(*a*) Distribution of the *ROSAT* PSPC (*solid line histogram*) and *Einstein* IPC (*dashed line histogram*) photon indices for 13 FSRQs at $z < 1$. The two distributions are different at $\sim$99% confidence according to the Kolmogorov-Smirnov test. The average IPC slope, $\langle \Gamma_{\rm IPC} \rangle = 1.48$ ($\sigma = 0.37$), is flatter than the average PSPC slope, $\langle \Gamma_{\rm PSPC} \rangle = 1.93$ ($\sigma = 0.27$), indicating the onset of a flat tail above $\approx$1 keV. (*b*) Confidence contours at 90% level for two parameters of interest from the maximum likelihood test, confirming that the 13 FSRQs have flatter IPC slopes than in the *ROSAT* range.

than HBLs, although with a large overlap of observed slopes.

5.2. *X-Ray Luminosity*

Figure 6*c* compares the distributions of the *ROSAT* luminosity densities at 1 keV of FSRQs (*solid line*; the subgroup at $z > 1$ is shown as shaded area) to those of HBLs and LBLs (*dotted and dashed lines*, respectively). The luminosities have been *K*-corrected multiplying the flux by $(1 + z)^{\alpha - 1}$, where α is the *ROSAT* energy index.

The distributions for HBLs and LBLs are not demonstrably different, with $P_{\rm KS} \sim 74\%$. The average X-ray luminosities of the two classes are reported in part B of Table 4, together with the luminosities of FSRQs and the low- and high-*z* FSRQ subgroups. (No weighted mean luminosities could be calculated for HBLs and LBLs, since the uncertainties on the 1 keV fluxes of these objects were not always provided in the quoted papers.)

The distribution for FSRQs, both for low- and high-*z* subgroups, is different from HBLs and LBLs at $P_{\rm KS} \gtrsim 99.99\%$. At all redshifts, FSRQs are on average more X-ray luminous than the BL Lacs by 1 order of magnitude, $\langle \log L_{1\ {\rm keV}} \rangle \sim 28$ erg s^{-1} Hz^{-1} for FSRQs versus $\langle \log L_{1\ {\rm keV}} \rangle \sim 27$ erg s^{-1} Hz^{-1} for both HBLs and LBLs (Table 4, part B).

As with the slope distribution in Figure 6*a*, note in Figure 6*c* the large overlap of the luminosity distributions among the three blazar classes, with several FSRQs having X-ray luminosities similar to both HBLs and LBLs.

6. SUMMARY OF THE OBSERVATIONAL RESULTS

We have presented the soft X-ray properties of 41 FSRQs observed with the *ROSAT* PSPC in pointed mode. The principal results of our analysis are the following:

1. FSRQs repeatedly observed with *ROSAT* exhibit flux variability with amplitude not larger than a factor of 2 on timescales of months/years, with little or no accompanying spectral variations. Typical variability amplitudes are on the order of 30% or less.
2. The *ROSAT* spectra of FSRQs are well described by a single power law plus Galactic absorption. Spectral flattening/softening is present in a small fraction only (3%–4%) of the sources. Spectral flattening can be equally modeled by excess absorption and by a convex continuum with strong ($\Delta\Gamma \gtrsim 1$) curvature, while soft excess flux is described in terms of a steep power law, a $\sim$60 eV blackbody, or a power law plus an absorption edge (the latter model is preferred in 1034−293).
3. The *ROSAT* photon index distribution of FSRQs spans a wide range, $0.5 \lesssim \Gamma \lesssim 2.5$; this spread is only in part accounted for by the anticorrelation of the slope with redshift. The intrinsic dispersion is larger at soft energies than at hard energies (rest frame), indicating a variety of spectral shapes at $\lesssim$a few keV
4. Thirteen FSRQs previously observed with the *Einstein* IPC (0.3–4.5 keV) have hard X-ray spectra flatter on average than with *ROSAT*, suggesting the emergence of a flat tail above $\approx$1 keV.
5. FSRQs have rest-frame slopes at soft X-rays fully consistent with LBLs and flatter than HBLs. However, a large overlap of observed photon indices is present among the three classes, with several FSRQs having HBL-like spectra.
6. FSRQs are intrinsically brighter by 1 order of magnitude than HBLs and even LBLs, while both BL Lacs types have similar X-ray luminosities. Again, a large overlap is present among the three classes.

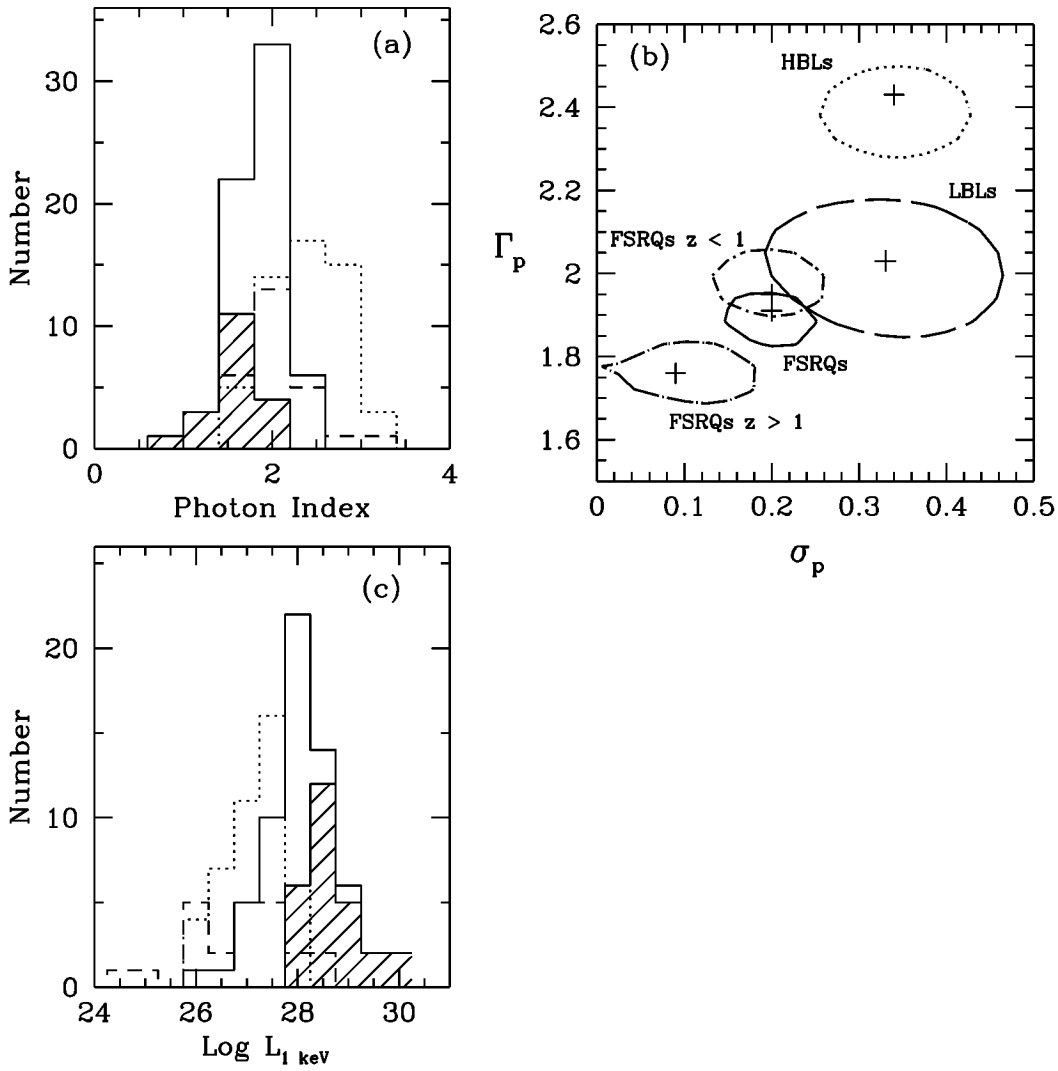

FIG. 6.—(*a*) Distribution of the *ROSAT* photon indices for FSRQs (*solid line*), HBLs (*dotted line*), and LBLs (*dashed line*). The solid line open histogram represents the total sample of FSRQs, while the shaded histogram represents the subgroup of $z > 1$ FSRQs. The slopes of FSRQs are indistinguishable from LBLs and flatter than HBLs. Note the overlap between the distributions of FSRQs and HBLs. (*b*) Confidence contours at 90% level for two parameters of interest from the maximum likelihood analysis for the different blazar classes, confirming that FSRQs and LBLs have very similar *ROSAT* spectra, flatter than HBLs. (*c*) Distributions of the *ROSAT* luminosity densities at 1 keV. Line types as in (*a*). Although on average FSRQs are intrinsically X-ray brighter than both HBLs and LBLs by 1 order of magnitude, several FSRQs have luminosities similar to BL Lacs.

7. DISCUSSION

7.1. *Soft X-Ray Continua of FSRQs*

One of the new results of this work is the finding that FSRQs have a wide distribution of *ROSAT* photon indices, $\Gamma \sim 0.5$–2.5, with a spread only in part due to a trend with the redshift. As is apparent from Figure 4*a*, for a given redshift at $z < 1$ there still is a large variety of spectral slopes, with objects having continua as flat as $\Gamma \sim 1.5$ and as steep as $\Gamma \sim 2.5$ (see also Fig. 3*b*). A similar spread of *ROSAT* spectral indices was found by Padovani et al. (1997); their sample of 90 FSRQs has an average photon index $\langle \Gamma \rangle = 2.09$ (weighted mean) and an observed dispersion of values in the range 0–3.

Brunner et al. (1994) studied the *ROSAT* spectra of a small sample of FSRQs (eight, six of which are at $z > 1$) from the S5 survey and reported an average slope $\langle \Gamma \rangle = 1.60$ with dispersion $\sigma = 0.56$. The *ROSAT* slopes of this sample are anticorrelated with the redshift (Urry et al. 1996); two objects at $z < 1$ have slopes $\Gamma \sim 2$, while the six objects at $z > 1$ have $\langle \Gamma \rangle = 1.33$, $\sigma = 0.47$. These average numbers are in agreement with our values in part A of Table 4 (note that the Brunner et al. objects are included in our sample). Comastri et al. (1997) have studied the *ROSAT* spectra of a group of 15 γ-ray–loud FSRQs, finding an average photon index $\langle \Gamma \rangle = 1.63$ and dispersion $\sigma = 0.36$. Splitting their sample into eight FSRQs at $z \lesssim 1$ and seven FSRQs at $z > 1$, we find $\langle \Gamma_{z<1} \rangle = 1.87$ ($\sigma = 0.20$) and $\langle \Gamma_{z>1} \rangle = 1.41$ ($\sigma = 0.34$), in agreement within 1 σ of our values in Table 4.

Flatter spectra are reported from studies at X-ray energies harder than the *ROSAT* PSPC. The *Einstein* IPC (0.3–4.5 keV) spectra of 12 HPQs, all at redshifts $\lesssim 1$, and of 19 FSRQs ($0.2 < z < 3.4$) both have a narrow distribution of photon indices centered at $\Gamma = 1.5$, with zero intrinsic dispersion (Worrall & Wilkes 1990). Flat slopes, in the range $\Gamma \sim 1.2$–1.7, were also found from the *EXOSAT* (0.1–10 keV) spectra of a small group of five FSRQs (Sambruna et

al. 1994a). The *GINGA* (2–20 keV) spectra of eight objects have somewhat steeper spectra, $\langle\Gamma\rangle = 1.76$ ($\sigma = 0.33$), although the signal-to-noise ratio is poor for several objects in this sample (Ohashi et al. 1989).

The variety of *ROSAT* spectral shapes we measure for FSRQs indicates that different mechanisms contribute to the soft X-rays in these sources. Steep ($\Gamma \gtrsim 2$) X-ray spectra, like those measured for HBLs, are associated to the high-energy tail of the synchrotron process, while the flatter spectra of LBLs are consistent with an inverse Compton component contributing significantly at these energies (see § 1). Since most FSRQs have *ROSAT* slopes similar to LBLs, the inverse Compton scattering is the most likely origin for the soft X-rays in these objects. This interpretation is supported by the analysis of the multifrequency continuum in the case of 3C 279 and 3C 345, which were monitored at radio, millimeter, and optical frequencies simultaneously with *ROSAT* (Grandi et al. 1996; Unwin et al. 1997).

What is remarkable, however, is that several FSRQs have steep, HBL-like *ROSAT* spectra, which suggest a synchrotron origin. Objects with steep ($\Gamma > 2$) *ROSAT* spectra include 0405−123, 0736+017, 0923+392, 0954+554, 1055+018, 1150+497, and 2155−152. Indication for spectral convexity, although not statistically significant, is present for 0736+017 and 1150+497 (§ 4.2.1). The average α_{rx}, α_{ro} indices of these seven objects, $\langle\alpha_{rx}\rangle = 0.85$ ($\sigma = 0.06$) and $\langle\alpha_{ro}\rangle = 0.66$ ($\sigma = 0.14$), are rather typical of FSRQs, while their α_{ox}, $\alpha_{ox} - \alpha_x$ indices ($\langle\alpha_{ox}\rangle = 1.23$, $\sigma = 0.16$ and $\langle\alpha_{ox} - \alpha_x\rangle = 0.0$, $\sigma = 0.13$) are flatter than FSRQs and intermediate between HBLs and LBLs (Sambruna et al. 1996). A first simple step could be to observe these sources with SAX to confirm the steep X-ray continua and put limits on the Compton component.

Similarly, a large spread is apparent from the distribution of X-ray luminosities of the three blazar classes (Fig. 6*c*). While FSRQs are, on average, more luminous than both LBLs and HBLs, a large overlap is present, with several FSRQs having 1 keV luminosity densities similar to BL Lacs. A large overlap of continuum properties is also present at lower frequencies. When plotted in color-color diagrams, FSRQs and LBLs occupy similar regions, while HBLs appear to segregate in the region of flatter radio-to-optical and optical-to-X-ray flux ratios (Brinkmann et al. 1996; Sambruna et al. 1996). However, the three blazar classes blend together smoothly, with several LBLs and FSRQs intruding in the HBL domain (see, e.g., Fig. 5 of Padovani et al. 1997). A continuity is also present in the luminosity of the optical emission lines; recent optical spectroscopy of large samples of FSRQs and BL Lacs (LBLs and HBLs) in a matching redshift range shows that the distribution of the line luminosity is continuous going from LBLs to FSRQs, with the latter objects clustered at higher values (Scarpa & Falomo 1997). Moreover, the line luminosity is correlated with the jet power, providing a physical link between the jet, where the continuum is produced, and the gaseous environment (Celotti, Padovani, & Ghisellini 1997).

These results reinforce the conclusion that a continuity of properties exists within the blazar class, with FSRQs, LBLs, and HBLs forming a unique population, where the same emission processes are at work on different physical scales (Sambruna et al. 1996). It may be expected that more sensitive surveys in the future will go deeper into the parameter space, further filling the gaps between the classes.

7.2. *X-Ray Variability of FSRQs*

FSRQs repeatedly observed with *ROSAT* on timescales of months/years exhibit flux variations with amplitudes not larger than a factor of 2, and with typical amplitudes of the order of $\lesssim$30%. No variations on shorter timescales were detected.

The X-ray variability of FSRQs at soft X-rays appear similar to other radio-loud (nonblazar) quasars. A study with the *Einstein* observatory led to the conclusion that flux variability on timescales $\lesssim$1 day is uncommon in radio-loud quasars, and that on longer timescales (6–18 months) typical variability amplitudes are of the order of 20%–60% amplitude (Zamorani et al. 1984). Two FSRQs in the *Einstein* sample, 3C 279 and 2223−052, are reported to have flux variations of 48% and 37% on timescales of less than 1 day, not different to other quasars (Zamorani et al. 1984). At higher X-ray energies, only a few objects have been repeatedly observed. Two *ASCA* (0.6–10 keV) spectra of 0528+134 taken seven months apart show an increase of the flux by a factor of 4 with no significant spectral changes; no variability is observed on short timescales within each $\sim$20 ks *ASCA* exposure (Sambruna et al. 1997). *GINGA* (2–15 keV) observations of 3C 279 show a decrease of a factor of 6 of the flux in 1 year, again with no spectral changes ($\Delta\Gamma \sim 0.1$; Ohashi et al. 1989), while recent *RXTE* observations detected a strong flare, with a factor of 3 increase of the flux in $\sim$6 days, simultaneous to EGRET (Wehrle et al. 1997). *EXOSAT* (0.1–10 keV) observations of Ton 599 show a variation of the flux of a factor of 2 in 1 year, again with constant spectral shape (Sambruna et al. 1994b). It appears that at higher X-ray energies the flux may vary with larger amplitudes than at lower X-ray energies, but again without spectral changes.

In contrast to FSRQs, both HBLs and LBLs exhibit large-amplitude flux variability in the X-rays, accompanied by correlated spectral changes. Luminosity variability up to a factor of 30 has been observed in HBLs, with several cases of doubling flux in 1 hour or so (Giommi et al. 1990). The variability is more pronounced at harder X-rays, with flatter spectra in the higher intensity state, consistent with the X-rays being produced by the highly variable tail of the synchrotron emission (Sembay et al. 1993; Sambruna et al. 1994a, 1995; Takahashi et al. 1997). In some LBLs, variability with amplitudes more than 100% amplitude on timescales of months were observed at soft X-rays, with flares of 80% changes in a few days in some cases (Giommi et al. 1990; Cappi et al. 1994; Madejski et al. 1996; Urry et al. 1996). The spectrum becomes steeper, $\Gamma \gtrsim 2$, during the higher intensity state. This is interpreted as the interplay of the highly variable synchrotron and the less variable flatter Compton tail, with the synchrotron component swamping the Compton tail during states of higher soft X-ray flux (Ulrich et al. 1997). It is worth mentioning that the LBLs where such a behavior has been observed are objects with spectral properties "intermediate" between LBLs and HBLs: their α_{rx} indices are in the range 0.7–0.9 (from Table 2 of Sambruna et al. 1996).

It is intriguing that the blazars with the highest X-ray luminosities display the lower amplitude variability. If confirmed, a trend of variability amplitude decreasing with increasing X-ray luminosity for blazars would be similar to Seyfert 1 objects (Nandra et al. 1997).

Finally, we note that in 3C 279 and 3C 345 the *ROSAT*

light curves track the behavior at radio to mm frequencies (Grandi et al. 1996; Unwin et al. 1997). This is commensurate with the X-rays arising via Compton upscattering off the same electron population responsible for emitting via synchrotron at radio to mm frequencies. A similar interpretation accounts for the low-amplitude variability at both millimeter and hard X-rays in 0528+134 (Sambruna et al. 1997).

7.3. *The High-energy Continuum of Emission-line Blazars*

The currently available data indicate that the average hard X-ray continuum of FSRQs flattens with respect to the extrapolation from the softer energies. Our comparison of the *ROSAT* PSPC (0.1–2.4 keV) and *Einstein* IPC (0.3–4.5 keV) slopes for 13 FSRQs indicates that a flat tail emerges at $\approx$1–2 keV rest-frame energies. A number of FSRQs are strong γ-ray emitters at MeV energies (Thompson et al. 1995), suggesting that their X-ray spectra must have an upturn somewhere. We identify the flat continuum connecting X-rays and γ-rays with the inverse Compton component (Maraschi et al. 1994; Madejski et al. 1996; Sambruna et al. 1997).

One of the still controversial issues concerning the high-energy continua of blazars is the origin of the seed photons that are upscattered at γ-ray energies. Competing scenarios include Compton upscattering of the synchrotron photons themselves off the relativistic electrons (synchrotron-self-Compton, SSC; Maraschi et al. 1992), and of the thermal photons produced outside the jet by the disk and/or the Broad Line Regions (external Compton, EC; Dermer et al. 1992; Sikora et al. 1994; Ghisellini & Madau 1996). Since the EC flux scales like the external radiation field it may be expected that this process becomes more and more important in stronger emission line blazars (e.g., Ghisellini & Maraschi 1993). The flux produced via Compton upscattering of external photons, F_C, is proportional to the external radiation density, W_{ext}, which in a first approximation can be measured from the luminosity and size of the broad emission line region: $F_C \propto \Gamma_B^6 W_{ext}$, where Γ_B is the Lorentz factor of the relativistic plasma in the jet. If $\Gamma_B \sim 10$ and does not vary widely (Ghisellini et al. 1993), and if the γ-ray emitting region is contained within a BLR of size $\lesssim 10^{18}$ cm (e.g., in 0528+134: Sambruna et al. 1997), the external radiation field becomes dominant over the synchrotron energy density (cf. eq. [1] of Ghisellini & Maraschi 1993). In this case, as the latter authors point out, the production of γ-rays occurs at the expense of the synchrotron emission at the lower frequencies, yielding higher ratios of the γ-ray to optical flux in blazars with more luminous emission lines.

Twelve FSRQs in our sample were detected at γ-rays with EGRET (Table 1); for seven of these objects published fluxes of broad emission lines (generally Mg II λ2798) were found in the literature. To these objects we add the two γ-ray–bright FSRQs 0454−234 and 1156+295 from the list of Dondi & Ghisellini (1995), and four LBLs with positive EGRET detections and broad emission lines (Stickel et al. 1993), for a total of 14 blazars detected at MeV energies. For these sources we constructed the γ-ray loudness parameter F_γ/F_{opt}, i.e., the ratio of the flux at $\geq$100 MeV, F_γ, and the optical flux in V band, F_{opt}. We also defined the ratio of the X-ray to the γ-ray fluxes, F_X/F_γ, describing the continuum between 1 keV and 100 MeV, and looked for trends of F_γ/F_{opt} and F_X/F_γ with the luminosity of the Mg II λ2798 line [1].

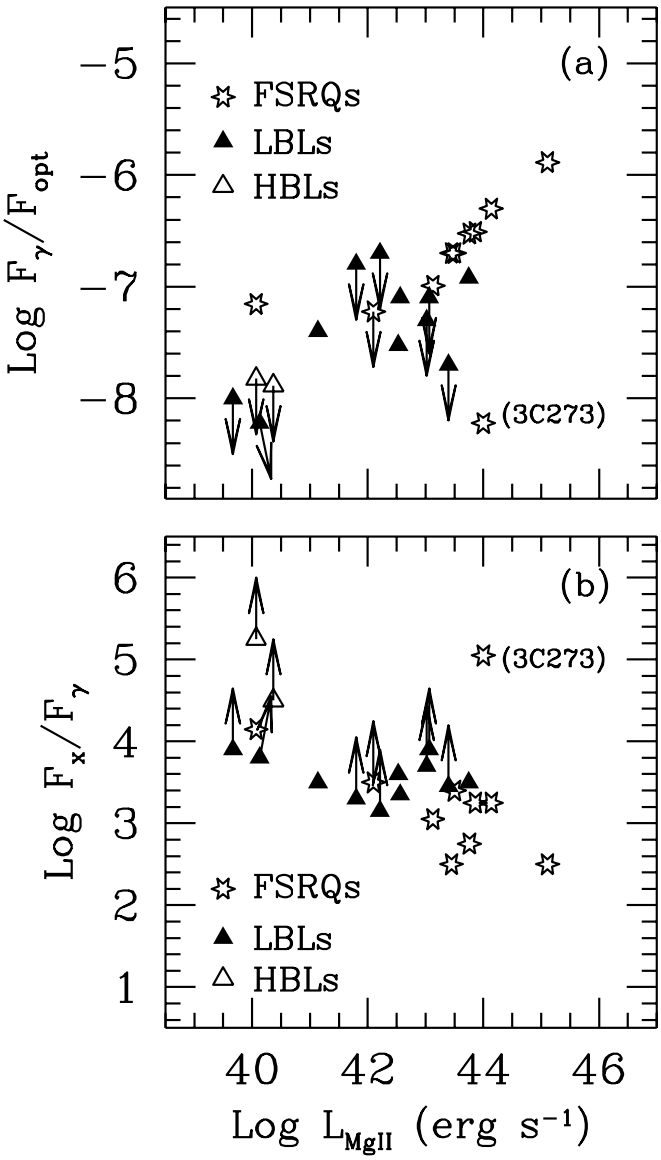

FIG. 7.—Plot of the Mg II λ2800 luminosity vs. (*a*) the γ-ray-to-optical flux ratio and (*b*) the X-ray-to-γ-ray flux ratio for the blazar classes. There is a trend for stronger emission line blazars to be more γ-ray–loud and to have flatter X-ray-to-γ-ray continua. Excluding the low-polarization blazar-like quasar 3C 273, in both panels the trends are significant at $\gtrsim$99%.

Figures 7*a* and 7*b* show the plot of F_γ/F_{opt} and F_x/F_γ versus the Mg II line luminosity, respectively, for FSRQs (*stars*) and LBLs (*filled triangles*). For reference, we also plotted upper limits for one FSRQ (3C 345), seven LBLs, and two HBLs that have not been detected yet at MeV frequencies and that have positive detections of the Mg II line. A trend is apparent in both Figures 7*a* and 7*b*, with objects having more luminous lines also being more γ-ray-loud. An exception is the low-polarization blazar-like

[1] In a few cases no Mg II fluxes were found in the literature. Instead of discarding these objects, we converted the fluxes of other published broad lines, generally Hα and C IV λ1549, to the flux of Mg II λ2798 using a conversion factor Mg II/H$\alpha \sim 0.33$ and Mg II/C IV ~ 0.25 derived from the UV and optical line compilations of Steiner (1981) and Wills et al. (1995).

quasar 3C 273, which has lower γ-ray-to-optical flux ratio and steeper X-ray-to-γ-ray continuum than predicted by its line luminosity. If 3C 273 is excluded, the trends in both Figures 7*a* and 7*b* are significant at $\sim$99.9% confidence from a survival analysis that takes into account the nondetections (correlation coefficients $\tau_{12} = 0.727$ and -0.729 for Figs. 7*a* and 7*b*, respectively). The line luminosity is correlated with the radio core power (Celotti et al. 1997) and with the redshift, as are $F_\gamma/F_{\rm opt}$ and F_x/F_γ (at $\gtrsim$97% confidence); after subtracting these quantities via a partial correlation analysis the trends in Figures 7*a* and 7*b* are still significant at $\sim$99% confidence ($\tau_{12,3} \gtrsim 0.5$). Figure 7 shows that the broad emission lines of blazars may have predictive power for the high-energy continuum, as expected in the context of EC models (e.g., Sikora et al. 1994).

8. CONCLUSIONS

We presented the soft X-ray properties of a large (41 objects) sample of FSRQs observed with the *ROSAT* PSPC in pointed mode. The 0.1–2.4 keV spectra are in general well described by a single power law with Galactic absorption, with spectral flattening/softening at the lower energies being present in only a small fraction (3%–4%) of objects. The *ROSAT* photon indices of FSRQs span the range 0.5–2.5, with a measurable intrinsic dispersion; the spread is only in part accounted for by a redshift effect.

FSRQs have soft X-ray slopes indistinguishable from low-energy peaked BL Lacs (LBLs) and flatter than high-energy peaked BL Lacs (HBLs) at rest-frame energies. This suggests that the emission mechanisms of the X-ray radiation in FSRQs and LBLs are very similar, with the inverse Compton process giving a significant contribution at these energies. However, contrary to the notion that FSRQs have "flat" spectra, several FSRQs have *ROSAT* photon indices as steep as HBLs, which suggests that a subgroup of the class may be synchrotron dominated. Similarly, FSRQs are on average intrinsically X-ray brighter than both LBLs and HBLs by 1 order of magnitude, but the luminosity distributions of the three blazar classes have a large overlap.

FSRQs repeatedly observed with *ROSAT* exhibit flux variations with amplitudes not larger than a factor of 2 on timescales of months/years, with little or no spectral changes and typical flux variations of 30% or less. This seems at odds with the larger amplitude flux and correlated spectral variations of the less luminous BL Lacs.

The *ROSAT* spectra of 13 FSRQs are steeper than their IPC (0.3–4.5 keV) spectra, indicating the onset of the flat Compton tail above $\approx$1–2 keV rest-frame energies. Examining correlations between the high-energy continuum and the luminosity of the broad emission lines in blazars, we find that objects with more luminous Mg II λ2798 lines have higher γ-ray-to-optical flux ratios and flatter X-ray-to-γ-ray continua. This is commensurate with the predictions of external Compton scattering models for the γ-rays.

This work was financially supported by an NRC Research Associate Fellowship at the NASA Goddard Space Flight Center. The author thanks Mike Eracleous, Laura Maraschi, Richard Mushotzky, Joe Pesce, Riccardo Scarpa, and Meg Urry for useful discussions and comments on the manuscript, and an anonymous referee for a valuable report. This research has made use of the NASA/IPAC Extragalactic Database (NED), which is operated by the Jet Propulsion Laboratory, California Institute of Technology, under contract with the National Aeronautics and Space Administration, and NASA's Astrophysics Data System Abstract Service.

APPENDIX

NOTES ON INDIVIDUAL SOURCES

0438−436.—Our results are in full agreement with Elvis et al. (1994). The excess absorption detected in the *ROSAT* spectra was confirmed in later *ASCA* observations, which seem to prefer a local absorber (Serlemitsos et al. 1994). The *ASCA* continuum is flat, with a photon index $\Gamma \sim 1.7$.

0528+134.—The *ROSAT* spectra of 0528+134 are consistent with a power law absorbed by a column density of $\approx 10^{22}$ cm^{-2}, in excess of the Galactic value, although within large uncertainties (Table 3 and Fig. 1; see also Zhang et al. 1994, Mukherjee et al. 1996). *ASCA* observations confirm the excess absorption over Galactic by $\Delta N_{\rm H} \approx 1 \times 10^{21}$ cm^{-2} (Sambruna et al. 1997). The *ASCA* continuum is flat, $\Gamma \sim 1.7$, and constant, despite the variation of a factor 4 of the flux between the two *ASCA* pointings taken 7 months apart. Several different scenarios are allowed by the *ASCA* data as to the location of the absorber (see Sambruna et al. 1997 for a discussion).

0836+710.—The free-$N_{\rm H}$ fit is preferred with a confidence $P_F > 99\%$ over the fixed (Galactic) $N_{\rm H}$ fit in both *ROSAT* spectra (comparing to the accurate estimate of Murphy et al. 1996). *ASCA* data obtained $\sim$5 months after *ROSAT* are consistent with column densities $\sim 1 \times 10^{21}$ cm^{-2}, larger than measured with *ROSAT*, thus suggesting variable absorption in this source (Cappi et al. 1997). The slope of the *ASCA* continuum is fairly similar to *ROSAT*, $\Gamma \sim 1.4$.

1034−293.—The fit with free-$N_{\rm H}$ yields a column density lower than the Galactic value, indicating a soft excess (Fig. 1). The presence of a soft excess was noted by Maraschi et al. (1995), who, however, fitted the data with a higher Galactic column density (4.7×10^{20} cm^{-2}). We fit the data with the more accurate column density of Murphy et al. (1996). The fits with both a broken power law and a power law plus blackbody are only marginally improved ($\Delta\chi^2 = 9$ for two additional parameters, $P_F < 90\%$) with respect to the fit with the power law plus Galactic $N_{\rm H}$. The fitted parameters for the broken power-law model are low-energy photon index $\Gamma_{\rm soft} \sim 3.0$, high-energy photon index $\Gamma_{\rm hard} = 1.34^{+0.38}_{-0.43}$, break energy $E_0 = 0.5^{+0.15}_{-0.31}$ keV, $\chi^2_r = 1.08/11$. The power law plus blackbody gives: temperature $kT = 0.04 \pm 0.02$ keV, photon index $\Gamma = 1.34^{+0.38}_{-0.47}$, $\chi^2_r = 1.09/11$. The fit with a power law plus Galactic $N_{\rm H}$ plus edge yields an improvement of $\Delta\chi^2 = 12.5$ ($P_F \sim 95\%$) for two additional parameters over the single power-law model, with the following parameters: $\Gamma = 1.96 \pm 0.18$, edge energy $E_e = 0.48^{+0.11}_{-0.21}$ keV, edge optical depth $\tau = 1.83(>0.9)$, $\chi^2_r = 0.83/11$. The best-fit edge energy is consistent with the K edge of O v ($E_{\rm rest} = 0.645$ keV) at the quasar's rest-frame.

3C 273.—This source is known for its strong and variable soft excess (Leach et al. 1995). The longest *ROSAT* archival exposure used here (Table 1) can equally be fitted by a concave broken power law ($\Gamma_{\rm soft} = 2.10^{+0.06}_{-0.04}$, $\Gamma_{\rm hard} = 1.87^{+0.04}_{-0.06}$, $E_0 = 0.64 \pm 0.15$ keV, $\chi^2_r = 1.06/181$), or by a power law plus Galactic $N_{\rm H}$ plus a blackbody of temperature $kT = 0.065^{+0.07}_{-0.014}$ keV, photon index $\Gamma = 1.82 \pm 0.06$, $\chi^2_r = 1.02/181$. Our results do not compare directly to Leach et al. (1995), who fixed the high-energy slope to 1.5, the value from the *GINGA* data. Fitting the data with a power law plus Galactic $N_{\rm H}$ plus edge yields a fit equivalent to the previous models, $\chi^2_r = 1.03/181$, with the following parameters: $\Gamma = 1.97 \pm 0.02$, $E_e = 0.54 \pm 0.05$, $\tau = 0.25 \pm 0.07$. The edge energy is consistent with the K edge of O II–VI in the quasar's rest frame.

3C 279.—*ROSAT* observed 3C 279 in 1992 January and in 1992 December/1993 January as part of a multifrequency campaign. As apparent in Table 2, the PSPC spectrum is in general well fitted by a single power law plus Galactic absorption. In a few cases, the fit with free $N_{\rm H}$ yields a significant improvement, with a fitted $N_{\rm H}$ slightly larger than Galactic. These include ROR 700981, 701104, 700987, 701119, 700988, and 700990. In the first four cases, however, the excess absorption seems due to a deficit of counts localized in the energy range 0.1–0.2 keV; when this energy range is excluded, the fitted column density is consistent with Galactic. In the remaining two cases (ROR 700988 and 700990), some extra absorption persists even after removing the softest energies. However, the extra absorption is small, $\Delta N_{\rm H} \lesssim 1 \times 10^{20}$ cm^{-2}. Given the still pending calibration issues of the PSPC, we conclude that the *ROSAT* spectrum of 3C 279 is well represented by a single power law with absorption consistent with Galactic, and photon index $\Gamma \sim 1.8$.

3C 345.—This source exhibits a strong "blue bump" in its optical/UV spectrum (Bregman et al. 1986), which can be modeled as a blackbody of temperature $\sim$a few eV contributing $\sim$15% of the total flux at 2500 Å (Smith et al. 1986, 1988). Fitting the *ROSAT* PSPC spectra of 3C 345 with a single power law with Galactic column density and photon index fixed to the value derived from IPC and *GINGA*, $\Gamma_{\rm hard} = 1.5$, a weak excess of soft counts ($\approx 1\ \sigma$) is present at energies $\lesssim$0.6 keV in all observations in Table 1. The addition of a blackbody model improves the fit with respect to a single power law in the case of observations 2, 3, and 4, at a confidence level of $P_F \sim 95\%$, 99%, and 95%, respectively ($\Delta\chi^2 = 4.5$, 11.6, 5.4, respectively, for two additional parameters). The blackbody has a fitted temperature around 70–100 eV, much higher than the temperature inferred for the UV bump, and contributes 17%–28% of the total 0.1–2.4 keV flux. The blackbody is preferred to a steep power law. Broadband X-ray spectra are necessary to confirm the presence of a soft excess in 3C 345 and study its nature.

Located 5′ away from the quasar is the low-luminosity ($L_{\rm X} \sim 5 \times 10^{41}$ ergs s^{-1}), nearby ($z = 0.03$) active galaxy NGC 6212, classified as Seyfert 1 on the basis of its broad optical emission lines (Halpern & Filippenko 1986).

Einstein IPC observations of NGC 6212 showed variability of the X-ray flux by a factor 4 on timescales of months (Halpern & Filippenko 1986). NGC 6212 was weakly detected in the three on-axis *ROSAT* PSPC images of 3C 345 (ROR 150014, 700869, 700870), with a count rate in 0.1–2.4 keV of $(7.3 \pm 1.8) \times 10^{-3}$, $(5.0 \pm 1.4) \times 10^{-3}$, and $(3.6 \pm 1.1) \times 10^{-3}$ count s^{-1}, respectively (from the algorithm SOSTA in XIMAGE). These count rates are at least an order of magnitude lower than the IPC count rates. This could be due to variability and/or, since the PSPC is sensitive to softer X-ray energies than the IPC, to excess absorption over Galactic (the Galactic absorption is very low along the direction to this object; 9×10^{19} cm^{-2}). Column densities as high as $\approx 10^{22}$ indeed were not ruled out by the IPC spectra (Halpern & Filippenko 1986).

1928+738.—The *ROSAT* spectrum of the nearby ($z = 0.302$) blazar 1928+738 shows evidence for excess absorption over Galactic (Table 3 and Fig. 1), whose origin is uncertain. No edgelike features are present in the *ROSAT* spectrum. The possible location of 1928+738 in a cluster of galaxies (Brunner et al. 1994, quoting Wagner, private communication) would suggest the soft X-ray absorber is associated to a cooling flow. Note that adding a Raymond-Smith model to the power law plus Galactic absorption improves the fit to the PSPC spectrum significantly ($\Delta\chi^2 = 91.2$). The fitted temperature is $kT \sim 0.9$ keV (for fixed solar abundances), and the power-law photon index becomes very flat, $\Gamma = 0.83^{+0.21}_{-0.37}$. 1928+738 is a strong UV and a candidate EUV emitter (Laor et al. 1995; Marshall, Fruscione, & Carone 1995), which rules out cold absorption along the line of sight. Spectroscopic follow-ups with current and future high-resolution missions are desirable to confirm and investigate the nature of the X-ray absorption in 1928+738.

2223−052.—This $z = 1.404$ quasar is located behind a damped Lyα system at $z_{\rm abs} = 0.4842$ with a column density of hydrogen of $N_{\rm H} \sim 7.9 \times 10^{20}$ cm^{-2} (Lanzetta et al. 1991). We performed joint fits to the two *ROSAT* spectra of 2223−052 (in order to increase the signal-to-noise ratio) with a single power law with two absorption column densities: one local, fixed to the Galactic value (Table 1), and the other absorber at $z = 0.4842$. The fit is good, $\chi^2_r = 1.06$ for 62 dof, and yields $N_{\rm H}(z_{\rm abs} = 0.4842) = 6.0^{+3.2}_{-2.8} \times 10^{20}$ cm^{-2}, consistent within the uncertainties with the value of Lanzetta et al. The fitted photon index is $\Gamma = 2.13 \pm 0.22$, consistent with the free-$N_{\rm H}$ fits in Table 3.

The *ROSAT* data can be used to derive constraints on the abundances of the lighter elements contributing to the absorption in the intervening system. At $z_{\rm abs} = 0.4842$, only the edges of carbon and oxygen are redshifted in the PSPC band. We fitted the PSPC data with a single power law absorbed by Galactic column density plus an absorber at $z = 0.4842$ with the abundances of carbon and oxygen free to vary. Because of the limited signal-to-noise ratio, only 90% confidence upper limits to the column densities could be derived. For carbon, $N_{\rm C} \lesssim 9 \times 10^{16}$ cm^{-2}, and for oxygen, $N_{\rm O} \lesssim 3 \times 10^{16}$ cm^{-2} (assuming a ratio of carbon to hydrogen and oxygen to hydrogen of 4.2×10^{-4} and 6.9×10^{-4}, respectively).

REFERENCES

Angel, J. R. P., & Stockman, H. S. 1980, ARA&A, 18, 321
Bania, T. M., Marscher, A. P., & Barvainis, R. 1991, AJ, 101, 2147
Bregman, J. N., et al. 1986, ApJ, 301, 708
Brinkmann, W., Siebert, J., Kollgaard, R. I., & Thomas, H.-C. 1996, A&A, 313, 356
Brunner, H., Lamer, G., Worrall, D. M., & Staubert, R. 1994, A&A, 287, 436
Cappi, M., Comastri, A., Molendi, S., Palumbo, G. C. C., Della Ceca, R., & Maccacaro, T. 1994, MNRAS, 271, 438
Cappi, M., Matsuoka, M., Comastri, A., Brinkmann, W., Elvis, M., Palumbo, G. G. C., & Vignali, C. 1997, ApJ, 478, 492
Celotti, A., Padovani, P., & Ghisellini, G. 1997, MNRAS, 286, 415
Comastri, A., Fossati, G., Ghisellini, G., & Molendi, S. 1997, ApJ, 480, 534
Dermer, C. D., Schlickeiser, R., & Mastichiadis, A. 1992, A&A, 256, L27
Dondi, L., & Ghisellini, G. 1995, MNRAS, 273, 583
Elvis, M., Fiore, F., Wilkes, B. J., McDowell, J., & Bechtold, J. 1994, ApJ, 422, 60
Elvis, M., Lockman, F. J., & Wilkes, B. J. 1989, AJ, 97, 777

Ghisellini, G., & Madau, P. 1996, MNRAS, 280, 67
Ghisellini, G., & Maraschi, L. 1993, in AIP Conf. Proc. 304, Proc. Second Compton Symp., ed. C. E. Fichtel, N. Gehrels, & J. P. Norris (New York: AIP), 616
Ghisellini, G., Padovani, P., Celotti, A., & Maraschi, L. 1993, ApJ, 407, 65
Giommi, P., Ansari, S. G., & Micol, A. 1995, A&AS, 109, 267
Giommi, P., Barr, P., Garilli, B., Maccagni, D., & Pollock, A. M. T. 1990, ApJ, 356, 432
Grandi, P., et al. 1996, ApJ, 459, 73
Halpern, J. P., & Filippenko, A. V. 1986, AJ, 91, 1019
Impey, C. D., & Tapia, S. 1988, ApJ, 333, 666
Kühr, H., & Schmidt, G. D. 1990, AJ, 99, 1
Kühr, H., Witzel, A., Pauliny-Toth, I. I. K., & Nauber, U. 1981, A&AS, 45, 367
Lamer, G., Brunner, H., & Staubert, R. 1996, A&A, 311, 384
Lanzetta, K. M., Wolfe, A. M., Turnshek, D. A., Lu, L., McMahon, R. G., & Hazard, C. 1991, ApJS, 77, 1
Laor, A., Bahcall, J. N., Jannuzi, B. T., Schneider, D. P., & Green, R. F. 1995, ApJS, 99, 1
Leach, C. M., McHardy, I. M., & Papadakis, I. E. 1995, MNRAS, 272, 221
Liszt, H. S., & Wilson, R. W. 1993, ApJ, 403, 663
Lockman, F. J., & Savage, B. D. 1995, ApJS, 97, 1
Madejski, G., Takahashi, T., Tashiro, M., Kubo, H., Hartman, R., Kallman, T., & Sikora, M. 1996, ApJ, 459, 156
Makino, F., et al. 1996, MPE Rep. 263, 413
Maraschi, L., Ciapi, A., Fossati, G., Tagliaferri, G., & Treves, A. 1995, ApJ, 443, 29
Maraschi, L., Ghisellini, G., & Celotti, A. 1992, ApJ, 397, L5
Maraschi, L., et al. 1994, ApJ, 435, L91
Marshall, H. L., Fruscione, A., & Carone, T. E. 1995, ApJ, 439, 90
Morrison, R., & McCammon, D. 1983, ApJ, 270, 119
Mukherjee, R., et al. 1996, ApJ, 470, 831
Murphy, E. M., Lockman, F. J., Laor, A., & Elvis, M. 1996, ApJS, 105, 369
Nandra, K., George, I. M., Mushotzky, R. F., Turner, T. J., & Yaqoob, T. 1997, ApJ, 476, 70
Nousek, J. A., & Lesser, A. 1993, *ROSAT* Newsletter, 8, 13
Ohashi, T., et al. 1989, in Proc. 23d ESLAB Symp. on Two Topics in X-Ray Astronomy, Vol. 2, AGN and the X-Ray Background (ESA SP-296), 837
Padovani, P. 1992, MNRAS, 257, 404
Padovani, P., & Giommi, P. 1996, MNRAS, 279, 526
Padovani, P., Giommi, P., & Fiore, F. 1997, MNRAS, 284, 569
Pauliny-Toth, I. I. K., Preuss, E., Witzel, A., Graham, D., Kellerman, K. I., & Ronnang, B. 1981, AJ, 86, 371
Pearson, T. J., & Readhead, A. C. S. 1988, ApJ, 328, 114
Perlman, E., Stocke, J. T., Wang, Q. D., & Morris, S. 1996, ApJ, 465, 1010
Reynolds, C. 1997, MNRAS, 286, 513
Sambruna, R. M., Barr, P., Maraschi, L., Tagliaferri, G., & Treves, A. 1994a, ApJ, 434, 468
———. 1994b, ApJS, 95, 371
Sambruna, R. M., Maraschi, L., & Urry, C. M. 1996, ApJ, 463, 444
Sambruna, R. M., et al. 1997, ApJ, 474, 639
Sambruna, R. M., Urry, C. M., Ghisellini, G., & Maraschi, L. 1995, ApJ, 449, 567
Scarpa, R., & Falomo, R. 1997, A&A, submitted
Schartel, N., Walter, R., Fink, H. H., & Truemper, J. 1996, A&A, 307, 33
Sembay, S., et al. 1993, ApJ, 404, 112
Serlemitsos, P., Yaqoob, T., Ricker, G., Woo, J., Kunieda, H., Terashima, Y., & Iwasawa, K. 1994, PASJ, 46, L43
Siemiginowska, A., Kuhn, O., Martin, E., Fiore, F., McDowell, J., & Wilkes, B. J. 1995, ApJ, 454, 77
Sikora, M., Begelman, M. C., & Rees, M. J. 1994, ApJ, 421, 153
Smith, P. S., Balonek, T. J., Heckert, P. A., & Elston, R. 1986, ApJ, 305, 484
Smith, P. S., Elston, R., Berriman, G., Allen, R. G., & Balonek, T. J. 1988, ApJ, 326, L39
Stark, A. A., Gammie, C. F., Wilson, R. W., Bally, J., Linke, R. A., Heiles, C., & Hurwitz, M. 1992, ApJS, 79, 77
Steiner, J. E. 1981, ApJ, 250, 469
Stickel, M., Fried, J. W., & Kühr, H. 1993, A&AS, 98, 393
Takahashi, T., et al. 1997, ApJ, 470, L89
Thompson, D. J., et al. 1995, ApJS, 101, 259
Ulrich, M.-H., Maraschi, L., & Urry, C. M. 1997, ARA&A, 35, 445
Unwin, S. C., Wehrle, A. E., Lobanov, A. P., Zensus, J. A., Madejski, G. M., Aller, M. F., & Aller, H. D. 1997, ApJ, 480, 596
Urry, C. M., & Padovani, P. 1995, PASP, 107, 803
Urry, C. M., Sambruna, R. M., Worrall, D. M., Kollgaard, R. I., Feigelson, E. D., Perlman, E. S., & Stocke, J. T. 1996, ApJ, 463, 424
Wall, J. V., & Peacock, J. A. 1985, MNRAS, 216, 173
Wehrle, A. E., et al. 1997, in preparation
Wills, B. J., et al. 1995, ApJ, 447, 139
Wills, B. J., Netzer, H., Uomoto, A. K., & Wills, D. 1980, ApJ, 237, 319
Worrall, D. M. 1989, in AGN and the X-Ray Background, ed. N. E. White (ESA-SP 296), 303
Worrall, D. M., & Wilkes, B. J. 1990, ApJ, 360, 396
Zamorani, G., Giommi, P., Maccacaro, T., & Tananbaum, H. 1984, ApJ, 278, 28
Zhang, Y. F., Marscher, A. P., Aller, H. D., Aller, M. F., Terasrranta, H., & Valtaoja, E. 1994, ApJ, 432, 91